AIMS Mathematics, 11(7): 19400–19439.
DOI: 10.3934/math.2026788
Received: 23 April 2026
Revised: 10 June 2026
Accepted: 11 June 2026
Published: 01 July 2026

https://www.aimspress.com/journal/Math

Research article

Spatial heterogeneity and nonlinear transmission drive tuberculosis hotspots: a reaction–diffusion modeling study

Olumuyiwa James Peter[1,2,*], Azhar Iqbal Kashif Butt[3,*], Sharifah Sakinah Syed Ahmad[4] and Fatemah H. H. Al Mukahal[3]

[1] Department of Mathematics, Saveetha School of Engineering, SIMATS, Saveetha University, Chennai, Tamil Nadu, India

[2] Department of Mathematical and Computer Sciences, University of Medical Sciences, Ondo, Ondo State, Nigeria

[3] Department of Mathematics and Statistics, College of Science, King Faisal University, Al-Ahsa 31982, Saudi Arabia

[4] Faculty of Artificial Intelligence and Cyber Security, Universiti Teknikal Malaysia Melaka, Malaysia

* **Correspondence:** Email: peterjames4real@gmail.com; aikhan@kfu.edu.sa.

Abstract: Tuberculosis remains a major public health challenge because of its long latent period, incomplete vaccine protection, and spatially heterogeneous transmission. This study develops a reaction–diffusion model incorporating vaccination, latent infection, active disease, treatment, recovery, nonlinear transmission, and population movement. Analytical and numerical investigations examine disease persistence, spatial spread, pattern formation, and control strategies. Results show that spatial heterogeneity and mobility can increase disease persistence and generate localized hotspots, transmission corridors, and clustered outbreaks. Numerical simulations demonstrate that interventions targeted at high-transmission areas reduce disease burden more effectively than uniformly distributed controls under the same resource constraints. These findings highlight the importance of spatial structure in tuberculosis dynamics and support geographically targeted vaccination and treatment strategies for improved disease control.

Keywords: tuberculosis; reaction–diffusion; Holling type II incidence; spatial heterogeneity; Turing instability; optimal control; BCG vaccination
Mathematics Subject Classification: 26A33, 34A08, 34A23, 92A25

1. Introduction

Tuberculosis (TB), caused by the bacterium *Mycobacterium tuberculosis*, is one of the deadliest infectious diseases worldwide, ranking among the leading causes of death from a single infectious agent [1–4]. Yet, despite the development of effective chemotherapy regimens and the long history of vaccine use, it remains responsible for more than a million deaths and infects tens of millions of people worldwide every year [1, 5, 6]. The persistence of tuberculosis is largely influenced by socioeconomic disparities, HIV coinfection, antibiotic resistance, and heterogeneous patterns of contact, which maintain high transmission rates in many high-burden countries [3, 7, 8]. In addition, the long latent period of infection, partial immunity following infection or vaccination, reinfection, and treatment-dependent recovery all contribute to the nonlinear and biologically complex dynamics of TB transmission [9–13].

One of the major characteristics of the epidemiology of tuberculosis is that most infected people remain latent, and only a small percentage ever become active [13]. Research on a large scale has shown that both endogenous reactivation and exogenous reinfection play an important part, particularly when the incidence of tuberculosis is high [12, 14, 15]. The long incubation period and the fact that people can be reinfected after recovering from the disease have significant consequences for the spread of tuberculosis [16–18]. Although the Bacillus Calmette–Guérin (BCG) vaccine can protect against severe forms, it does not completely protect against infection or the spread of the disease, and the level of protection can vary greatly from one population to another [19–22]. Research, both controlled and natural, has shown that the BCG vaccine can protect against the progression from infected to ill, but not against the initial acquisition of the infection, which means that the long latent periods continue to be a source of long-term persistence of tuberculosis [5, 13, 21].

Mathematical models have been critical in piecing together the dynamics of tuberculosis, measuring the transmissibility of the disease, and evaluating control strategies [23–25]. The basic models used for tuberculosis have been the susceptible–latent–infected–recovered (SLIR) and susceptible–latent–infected–recovered–with–vaccine–and–treatment (SLIRVT) models [16, 18]. However, for more realistic models, other factors have to be taken into account [17, 26].

In high-burden settings, TB transmission does not increase linearly with the number of infectious individuals because of contact saturation, behavioral changes, and limitations in diagnosis and care. Nonlinear incidence functions, particularly Holling type II (saturated) incidence, are suitable for describing TB transmission in such settings [27–29]. Saturated incidence has been shown to produce backward bifurcation, bistability, and complex threshold behavior in TB models [28, 30].

Spatial heterogeneity is another defining feature of TB. Urbanization, migration, socioeconomic inequality, and heterogeneous contact patterns lead to strong spatial variation in TB prevalence [1, 2]. Reaction–diffusion models provide a powerful framework for studying the spatiotemporal spread of infectious diseases [31, 32]. When combined with nonlinear transmission and differential mobility of population groups, such models can exhibit diffusion-driven (Turing) instabilities, generating spatial patterns such as TB hotspots, stripes, and clusters [29, 31, 33, 34].

Spatial pattern formation in TB can be interpreted epidemiologically as persistent foci of infection, including urban slums, prisons, and mining communities, where transmission is amplified [29, 35]. Understanding how such patterns arise is therefore crucial for designing effective TB control strategies.

The theory of optimal control provides an excellent framework for determining how to apportion

scarce public health resources so that the effect of the disease is minimized [36,37]. In the world of TB modeling, individuals have used the theory of optimal control to determine appropriate vaccination, screening, and treatment strategies that evolve over time [38, 39]. Recently, the concepts have expanded to include space, so that appropriate interventions can be designed that evolve over time and location [35, 40].

As a result of the need to understand the effects of nonlinear transmission, geography, and movement of individuals on the spread of TB, a novel framework for spatiotemporal modeling is presented. In other words, the classic theory of TB is extended to include a spatially structured, nonlinear framework. The main novel aspects of the current research are:

- A six-compartment reaction–diffusion model of TB transmission that integrates BCG vaccination, latent infection, active disease, chemotherapy, and recovery with spatial diffusion, allowing for the joint analysis of epidemiological and spatial dynamics.
- Incorporation of Holling type II (saturated) transmission into a spatial reaction–diffusion tuberculosis model, enabling the investigation of contact saturation, behavioral responses, and diagnostic constraints in high-prevalence settings.
- A spatially structured transmission environment where local TB transmission rates are spatially distributed according to an urban–rural population density profile, facilitating the explicit analysis of TB risk differences and hotspots.
- The construction of a spatial basic reproduction number, R_0^S, using a next-generation operator approach for reaction–diffusion systems, providing a rigorous link between TB invasion and persistence and the spectral properties of spatially distributed transmission and mobility.
- A rigorous proof that $R_0^S \geq R_0$, demonstrating that spatial heterogeneity and diffusion can maintain TB even when a well-mixed model predicts TB elimination.
- The derivation of diffusion-driven (Turing) instability conditions for TB transmission with saturated incidence, proving that different movement rates between latent and infectious individuals can lead to the instability of a uniform endemic equilibrium and the emergence of persistent spatial patterns of TB.
- The first numerical study to demonstrate that nonlinear TB transmission and mobility dynamics alone can generate endemic hotspots, transmission corridors, and clustered outbreaks, providing a mechanistic explanation for observed spatial heterogeneity in TB.
- The incorporation of spatially targeted vaccination and treatment strategies into a pattern-forming TB model, demonstrating that hotspot-targeted control strategies are more effective than uniform control strategies under the same resource constraints.

This study offers a fundamentally new understanding of how tuberculosis hotspots form and how they can be best managed in spatially structured populations by integrating nonlinear transmission, spatial heterogeneity, diffusion-driven instability, and targeted intervention within a single mathematical framework. The remaining sections of this work are organized as follows. In Section 2, we present a model for tuberculosis that accounts for regional heterogeneity and includes nonlinear saturation transmission and diffusion. Section 3 sets the fundamental mathematical features of the model, including its positivity, boundedness, and well-posedness. Section 4 analyzes nonspatial (ordinary differential equations (ODE)) dynamics, such as disease-free and endemic equilibria and the basic reproduction number R_0. In Section 5, we analyze the spatial model and obtain the spatial

reproduction number R_0^S. We also prove the existence and stability of spatial steady states and provide criteria for diffusion-driven (Turing) instability. Section 6 provides numerical simulations of hotspot formation and assesses the effectiveness of geographically targeted vaccination and treatment techniques. Section 7 highlights key findings and examines their epidemiological implications.

2. Model formulation

We propose a spatiotemporal model to capture the spread of tuberculosis (TB). TB is a chronic contagious respiratory disease characterized by long latent periods, the possibility of recovery based on treatment, and the chance of being reinfected. Our model seeks to capture both the biological process of TB and the effect of spatial heterogeneities, driven by urbanization and geographical factors.

We examine the transmission of tuberculosis in a spatially heterogeneous region Ω in the plane, $\Omega \subset \mathbb{R}^2$. Six sections are created based on the health state of the population. Let [H(x,t), B(x,t), Q(x,t), Y(x,t), C(x,t), Z(x,t)] represent the densities of TB-free individuals, BCG-vaccinated individuals, latently infected individuals, active TB patients, chemotherapy patients, and recovered individuals, respectively, at spatial position $x \in \Omega$ and time $t \geq 0$.

Therefore,

$$M(x,t) = H(x,t) + B(x,t) + Q(x,t) + Y(x,t) + C(x,t) + Z(x,t) \tag{2.1}$$

is the overall population density at any location x and time t. The description of the state variables H, B, Q, Y, C, Z is given in Table 1.

Table 1. State variables of the TB model.

Variable	Description
$H(x,t)$	TB-free individuals
$B(x,t)$	BCG-vaccinated individuals
$Q(x,t)$	Latent TB carriers
$Y(x,t)$	Active TB patients
$C(x,t)$	Individuals on chemotherapy
$Z(x,t)$	Recovered individuals
$M(x,t)$	Total population

2.1. Model assumptions

The model is constructed based on the following assumptions:

(1) TB transmission occurs through close and prolonged contact with infectious individuals.
(2) At low prevalence, transmission increases approximately linearly, whereas at high prevalence, it saturates due to behavioral changes and case detection.
(3) BCG vaccination provides partial protection against TB infection.
(4) Newly infected individuals enter a latent stage before becoming infectious.
(5) Latent individuals may progress to active TB.
(6) Infectious individuals may begin chemotherapy.
(7) Successfully treated individuals recover but remain susceptible to reinfection.
(8) Natural death affects all population classes equally.

(9) Recruitment enters exclusively the TB-free class. Individuals spread randomly over space.
(10) TB transmission differs geographically due to diverse urbanization and contact patterns.
(11) There is no population flux over the domain's boundaries.

2.2. Force of infection

Inspired by Holling type II saturation dynamics, the force of infection is defined in frequency–dependent form as

$$\Psi(x,t) = \theta(x)\frac{Y(x,t)}{M(x,t) + \omega Y(x,t)}, \tag{2.2}$$

where $\theta(x)$ is the spatially heterogeneous TB transmission rate, $M(x,t)$ is the total population density defined in (2.1), and $\omega > 0$ is the saturation coefficient reflecting contact limitation and diagnostic response. This formulation ensures that transmission depends on the prevalence of infectious individuals and remains bounded as $Y(x,t)$ increases. Functional responses of this type have been widely used in epidemic models to capture saturation effects in transmission, extending the classical bilinear incidence assumption [41]. The relevance of Holling-type mechanisms in tuberculosis-related modeling has also been demonstrated by Aggarwal et al. [42], who incorporated a Holling type II treatment rate in an HIV–TB coinfection framework.

2.3. Spatial heterogeneity

The spatial variance in contact possibilities resulting from baseline urbanization and settlement pattern is represented by the transmission rate $\theta(x)$, which is defined by

$$\theta(x) = \theta_0\left[1 + \eta\tanh\left(\frac{\xi(x) - \xi_0}{\Delta\xi}\right)\right], \tag{2.3}$$

where θ_0 is the baseline transmission rate, η measures the strength of heterogeneity, and $\xi(x)$ is a fixed background population density field describing urban–rural structure:

$$\xi(x) = \xi_{\min} + (\xi_{\max} - \xi_{\min})\exp\left(-\frac{|x - x^*|^2}{2\sigma_\xi^2}\right). \tag{2.4}$$

In the absence of spatial movement, the TB dynamics is governed by

$$\begin{aligned}
\frac{d_H}{dt} &= (1-\nu)\Pi - \Psi H - \delta H,\\
\frac{dB}{dt} &= \nu\Pi - (1-\epsilon)\Psi B - \delta B,\\
\frac{dQ}{dt} &= \Psi(H + (1-\epsilon)B) + \kappa\Psi Z - (\alpha+\delta)Q,\\
\frac{dY}{dt} &= \alpha Q - (\gamma + \tau + \delta)Y,\\
\frac{dC}{dt} &= \tau Y - (\rho + \delta)C,\\
\frac{dZ}{dt} &= \gamma Y + \rho C - \kappa\Psi Z - \delta Z,
\end{aligned} \tag{2.5}$$

where Ψ is defined in (2.2) and the description of the model parameters is given Table 2.

Table 2. Model parameters.

Parameter	Meaning
Π	Recruitment rate
ν	Fraction of newborns vaccinated with BCG
ϵ	Vaccine efficacy (degree of protection)
α	Progression from latent to active TB
τ	Rate of treatment initiation
ρ	Treatment success rate
γ	Rate of natural recovery
κ	Rate of reinfection susceptibility
δ	Natural mortality rate
ω	Saturation parameter
D_i	Diffusion coefficients

2.4. Reaction–diffusion TB model

Including spatial movement, the TB system becomes

$$\begin{aligned}
\frac{\partial H}{\partial t} &= D_H \Delta H + (1-\nu)\Pi - \Psi H - \delta H,\\
\frac{\partial B}{\partial t} &= D_B \Delta B + \nu\Pi - (1-\epsilon)\Psi B - \delta B,\\
\frac{\partial Q}{\partial t} &= D_Q \Delta Q + \Psi(H + (1-\epsilon)B) + \kappa\Psi Z - (\alpha+\delta)Q,\\
\frac{\partial Y}{\partial t} &= D_Y \Delta Y + \alpha Q - (\gamma+\tau+\delta)Y,\\
\frac{\partial C}{\partial t} &= D_C \Delta C + \tau Y - (\rho+\delta)C,\\
\frac{\partial Z}{\partial t} &= D_Z \Delta Z + \gamma Y + \rho C - \kappa\Psi Z - \delta Z,
\end{aligned} \tag{2.6}$$

with $\Psi(x,t)$ defined in (2.2) and $\theta(x)$ given by (2.3).

Homogeneous Neumann boundary conditions are imposed:

$$\frac{\partial H}{\partial n} = \frac{\partial B}{\partial n} = \frac{\partial Q}{\partial n} = \frac{\partial Y}{\partial n} = \frac{\partial C}{\partial n} = \frac{\partial Z}{\partial n} = 0, \quad x \in \partial\Omega, \tag{2.7}$$

together with non-negative initial conditions.

3. Mathematical analysis

This section describes the essential mathematical characteristics of the reaction–diffusion tuberculosis model (2.6)-(2.7). These characteristics ensure that the model is epidemiologically meaningful and mathematically well-posed. We begin by demonstrating that all population densities stay non-negative throughout time.

3.1. Positivity of solutions

Theorem 1. *Let the initial conditions satisfy*

$$H(x,0),\ B(x,0),\ Q(x,0),\ Y(x,0),\ C(x,0),\ Z(x,0) \geq 0, \qquad x \in \Omega.$$

Then the solution of the reaction–diffusion system (2.6) *subject to the boundary conditions* (2.7) *expressed as*

$$H(x,t),\ B(x,t),\ Q(x,t),\ Y(x,t),\ C(x,t),\ Z(x,t) \geq 0, \qquad \forall x \in \Omega,\ t > 0.$$

Proof. We write System (2.6) in vector form:

$$\frac{\partial \mathbf{U}}{\partial t} = D\Delta\mathbf{U} + F(\mathbf{U}), \qquad \mathbf{U} = (H, B, Q, Y, C, Z)^T,$$

where

$$D = \text{diag}(D_H, D_B, D_Q, D_Y, D_C, D_Z),$$

and $F(\mathbf{U}) = (F_H, F_B, F_Q, F_Y, F_C, F_Z)^T$ denotes the reaction terms.

We show that the reaction operator F is *quasi-positive*; that is, whenever one component is zero, and all others are positive, the corresponding reaction term is positive.

From (2.6), the reaction terms are

$$\begin{aligned}
F_H &= (1-\nu)\Pi - \Psi H - \delta H,\\
F_B &= \nu\Pi - (1-\epsilon)\Psi B - \delta B,\\
F_Q &= \Psi(H + (1-\epsilon)B) + \kappa\Psi Z - (\alpha+\delta)Q,\\
F_Y &= \alpha Q - (\gamma+\tau+\delta)Y,\\
F_C &= \tau Y - (\rho+\delta)C,\\
F_Z &= \gamma Y + \rho C - \kappa\Psi Z - \delta Z,
\end{aligned}$$

where $\Psi(x,t)$ is given by (2.2).

We now check quasi-positivity for each component:

- If $H = 0$, then
$$F_H\big|_{H=0} = (1-\nu)\Pi \geq 0.$$
- If $B = 0$, then
$$F_B\big|_{B=0} = \nu\Pi \geq 0.$$
- If $Q = 0$, then
$$F_Q\big|_{Q=0} = \Psi(H + (1-\epsilon)B) + \kappa\Psi Z \geq 0,$$
because $\Psi(x,t) \geq 0$ from (2.2).
- If $Y = 0$, then
$$F_Y\big|_{Y=0} = \alpha Q \geq 0.$$
- If $C = 0$, then
$$F_C\big|_{C=0} = \tau Y \geq 0.$$

- If $Z = 0$, then

$$F_Z\big|_{Z=0} = \gamma Y + \rho C \geq 0.$$

Thus, the reaction terms are quasi-positive.

The parabolic maximum principle is applicable when the diffusion operator is diagonal and the System (2.6) has homogeneous Neumann boundary conditions (2.7). Assume, for contradiction, that one component (say u) goes negative at the first moment $t^* > 0$ and point $x^* \in \overline{\Omega}$. Then

$$u(x^*, t^*) = 0, \qquad \partial_t u(x^*, t^*) \leq 0, \qquad \Delta u(x^*, t^*) \geq 0.$$

Thus, quasi-positivity means that

$$F_u(\mathbf{U}(x^*, t^*)) \geq 0.$$

Therefore,

$$\partial_t u - D_u \Delta u = F_u \geq 0,$$

which contradicts $\partial_t u \leq 0$ and $\Delta u \geq 0$. Thus, no component can become negative.

Therefore,

$$H(x,t),\ B(x,t),\ Q(x,t),\ Y(x,t),\ C(x,t),\ Z(x,t) \geq 0 \quad \text{for all } x \in \Omega,\ t > 0.$$

□

3.2. Boundedness and invariant region

We now prove that the overall population density is consistently bounded throughout time. This suggests that the model contains a biologically significant invariant region.

Thus, the total population is defined as (2.1) as

$$M(x,t) = H(x,t) + B(x,t) + Q(x,t) + Y(x,t) + C(x,t) + Z(x,t).$$

Adding all six equations of the reaction–diffusion system (2.6), we obtain

$$\begin{aligned}\frac{\partial M}{\partial t} &= D_H \Delta H + D_B \Delta B + D_Q \Delta Q + D_Y \Delta Y + D_C \Delta C + D_Z \Delta Z \\ &\quad + \Pi - \delta(H + B + Q + Y + C + Z).\end{aligned}$$

All transmission, progression, recovery, vaccination, and therapy phrases are canceled because they describe internal transfers between compartments.

Using (2.1), this reduces to

$$\frac{\partial M}{\partial t} = \nabla \cdot (D_H \nabla H + D_B \nabla B + D_Q \nabla Q + D_Y \nabla Y + D_C \nabla C + D_Z \nabla Z) + \Pi - \delta M. \tag{3.1}$$

Using the homogeneous Neumann boundary conditions (2.7) and integrating over Ω, the divergence term vanishes. Therefore, the spatially averaged total population satisfies

$$\frac{d}{dt} \int_\Omega M(x,t)\, dx = \Pi |\Omega| - \delta \int_\Omega M(x,t)\, dx.$$

Moreover, pointwise comparison with the ordinary differential equation

$$\frac{d\overline{M}}{dt} = \Pi - \delta\overline{M} \tag{3.2}$$

implies, by the parabolic comparison principle applied to (3.1), that

$$0 \le M(x,t) \le \overline{M}(t) \qquad \forall x \in \Omega,\ t > 0,$$

where $\overline{M}(t)$ solves (3.2) with $\overline{M}(0) = \sup_{x\in\Omega} M(x,0)$.

Solving (3.2) yields

$$\overline{M}(t) = \frac{\Pi}{\delta} + \Big(\overline{M}(0) - \frac{\Pi}{\delta}\Big)e^{-\delta t}.$$

Hence,

$$0 \le M(x,t) \le \frac{\Pi}{\delta} \qquad \forall x \in \Omega,\ t > 0.$$

Therefore, the set

$$\mathcal{D} = \Big\{(H,B,Q,Y,C,Z) \in \mathbb{R}^6_+ :\ 0 \le H + B + Q + Y + C + Z \le \tfrac{\Pi}{\delta}\Big\}$$

is a positively invariant and biologically meaningful region for System (2.6).

3.3. The reaction–diffusion TB model's well-posedness

The reaction–diffusion system (2.6)-(2.7) admits a single global classical solution that depends continuously on the starting data, as we demonstrate in this section.

3.3.1. Functional setting

Let

$$\mathbf{U}(x,t) = (H,B,Q,Y,C,Z)^T.$$

Define the Banach space

$$X = (C(\overline{\Omega}))^6, \qquad \|\mathbf{U}\|_X = \sum_{i=1}^{6} \|u_i\|_{C(\overline{\Omega})}.$$

Let the diffusion operator be

$$\mathcal{A}\mathbf{U} = \big(D_H\Delta H, D_B\Delta B, D_Q\Delta Q, D_Y\Delta Y, D_C\Delta C, D_Z\Delta Z\big)^T$$

with domain

$$D(\mathcal{A}) = \Big\{\mathbf{U} \in (C^2(\Omega)\cap C(\overline{\Omega}))^6 :\ \frac{\partial \mathbf{U}}{\partial n} = 0 \text{ on } \partial\Omega\Big\}.$$

It is well-known that $\mathcal{A}$ generates a strongly continuous analytic semigroup $e^{t\mathcal{A}}$ on X.

The System (2.6) can be written abstractly as

$$\frac{d\mathbf{U}}{dt} = \mathcal{A}\mathbf{U} + F(\mathbf{U}), \qquad \mathbf{U}(0) = \mathbf{U}_0, \tag{3.3}$$

where $F(\mathbf{U})$ is defined from (2.6).

3.3.2. Lipschitz property of the force of infection

Recall that

$$\Psi(x,t) = \theta(x)\frac{Y(x,t)}{M(x,t)+\omega Y(x,t)}, \qquad M = H + B + Q + Y + C + Z.$$

Define

$$g(Y,M) = \frac{Y}{M+\omega Y}.$$

For any bounded set

$$0 \le Y \le K, \qquad 0 \le M \le K,$$

we have

$$\frac{\partial g}{\partial Y} = \frac{M}{(M+\omega Y)^2}, \qquad \frac{\partial g}{\partial M} = -\frac{Y}{(M+\omega Y)^2}.$$

Because $M + \omega Y \ge \omega Y \ge 0$ and $M + \omega Y \ge M$, it follows that

$$\left|\frac{\partial g}{\partial Y}\right| \le \frac{K}{(\omega K)^2}, \qquad \left|\frac{\partial g}{\partial M}\right| \le \frac{K}{(\omega K)^2}.$$

Hence, $g(Y,M)$ is Lipschitz continuous on bounded sets. Because $\theta(x)$ is bounded from (2.3), $\Psi(x,t)$ is locally Lipschitz in $\mathbf{U}$.

Therefore, all components of $F(\mathbf{U})$ are locally Lipschitz in X.

3.3.3. Local existence and uniqueness

Equation (3.3) admits a unique local mild solution according to analytic semigroup theory for semilinear parabolic systems.

$$\mathbf{U} \in C([0,T_{\max}),X) \cap C^1((0,T_{\max}),X)$$

for some $T_{\max} > 0$.

3.3.4. Global existence

From the invariant region proved previously,

$$0 \le H, B, Q, Y, C, Z \le \frac{\Pi}{\delta},$$

so

$$\|\mathbf{U}(t)\|_X \le 6\frac{\Pi}{\delta}.$$

Hence, blow-up in finite time is impossible. Therefore,

$$T_{\max} = \infty,$$

and the solution is global.

3.3.5. Continuous dependence on initial data

Let $\mathbf{U}_1, \mathbf{U}_2$ be two solutions of (3.3) with initial data $\mathbf{U}_{1,0}, \mathbf{U}_{2,0}$. Then

$$\frac{d}{dt}(\mathbf{U}_1 - \mathbf{U}_2) = \mathcal{A}(\mathbf{U}_1 - \mathbf{U}_2) + F(\mathbf{U}_1) - F(\mathbf{U}_2).$$

Because F is Lipschitz on bounded sets, there exists $L > 0$ such that

$$\|F(\mathbf{U}_1) - F(\mathbf{U}_2)\|_X \leq L\|\mathbf{U}_1 - \mathbf{U}_2\|_X.$$

By Grönwall's inequality,

$$\|\mathbf{U}_1(t) - \mathbf{U}_2(t)\|_X \leq e^{Lt}\|\mathbf{U}_{1,0} - \mathbf{U}_{2,0}\|_X.$$

Thus, the solution depends continuously on the initial data.

This proves global existence, uniqueness, and continuous dependence for System (2.6).

4. ODE (nonspatial) dynamics

The well-mixed population case of the full reaction–diffusion model (2.6) corresponds to the spatially homogeneous tuberculosis model represented by the system of ordinary differential equations (2.5).

4.1. Disease-free equilibrium

The absence of tuberculosis in the population is correlated with the disease-free equilibrium (DFE). Consequently, we set

$$Q = Y = C = 0. \tag{4.1}$$

Substituting (4.1) into the ODE system (2.5) and using the definition of the force of infection (2.2), we have

$$\Psi = \theta\frac{Y}{M + \omega Y} = 0$$

because $Y = 0$. The remaining equations for H, B, and Z become

$$\frac{dH}{dt} = (1 - \nu)\Pi - \delta H, \tag{4.2}$$

$$\frac{dB}{dt} = \nu\Pi - \delta B, \tag{4.3}$$

$$\frac{dZ}{dt} = -\delta Z. \tag{4.4}$$

At equilibrium, all time derivatives vanish. Solving (4.2) gives

$$H^* = \frac{(1 - \nu)\Pi}{\delta}. \tag{4.5}$$

Substituting (4.5) into (4.3) and setting $dB/dt = 0$ yields

$$0 = \nu\Pi - \delta B^* \quad \Longrightarrow \quad B^* = \frac{\nu\Pi}{\delta}.$$

Finally, from (4.4), we obtain

$$0 = -\delta Z^* \quad \Longrightarrow \quad Z^* = 0.$$

Therefore, the disease-free equilibrium of System (2.5) is

$$\mathcal{E}_0 = (H^*, B^*, Q^*, Y^*, C^*, Z^*) = \left(\frac{(1-\nu)\Pi}{\delta}, \frac{\nu\Pi}{\delta}, 0, 0, 0, 0\right). \tag{4.6}$$

In the absence of tuberculosis transmission, this equilibrium depicts a population in which a percentage ν of infants receives a BCG vaccination, and the remainder fraction $(1-\nu)$ joins the TB-free class.

4.2. Basic reproduction number R_0

The basic reproduction number R_0 is defined as the expected number of secondary TB cases produced by a single infectious individual introduced into a population at the disease-free equilibrium, where a fraction ν of newborns are protected by BCG vaccination. This quantity determines whether tuberculosis can invade and persist in the population described by the ODE model. We compute R_0 using the next-generation matrix method [25, 43, 44].

4.2.1. Identification of infected compartments

The latent class Q and the infectious class Y are the epidemiological compartments linked to tuberculosis infection. The infected state vector is thus defined as

$$\Phi = (Q, Y)^T.$$

Let $\mathcal{F}_i(X)$ represent the rate at which new infections emerge in each infected compartment i, and $\mathcal{V}_i(X)$ represent the net rate at which persons are transferred out of compartment i by all other processes.

From the ODE model (2.5), these terms are

$$\mathcal{F}_Q = \Psi(H + (1-\epsilon)B) + \kappa\Psi Z, \qquad \mathcal{F}_Y = 0, \tag{4.7}$$

$$\mathcal{V}_Q = (\alpha + \delta)Q, \qquad \mathcal{V}_Y = (\gamma + \tau + \delta)Y - \alpha Q. \tag{4.8}$$

4.2.2. Linearization at the disease-free equilibrium

At the disease-free equilibrium (4.6),

$$H^* = \frac{(1-\nu)\Pi}{\delta}, \qquad B^* = \frac{\nu\Pi}{\delta}, \qquad Z^* = 0,$$

and the total population is

$$M^* = H^* + B^* = \frac{\Pi}{\delta}.$$

The force of infection (2.2) is

$$\Psi = \theta\frac{Y}{M + \omega Y}.$$

Linearizing near the DFE (where $Y = 0$) gives

$$\Psi \approx \theta \frac{Y}{M^*}.$$

Substituting into (4.7), we obtain

$$\mathcal{F}_Q = \theta \frac{Y}{M^*}\Big(H^* + (1-\epsilon)B^*\Big) = \theta \frac{Y}{M^*}\Big((1-\nu) + (1-\epsilon)\nu\Big)\frac{\Pi}{\delta}.$$

Hence the Jacobian matrices of $\mathcal{F}$ and $\mathcal{V}$ at the DFE are

$$\mathbf{F} = \begin{pmatrix} 0 & \dfrac{\theta(H^* + (1-\epsilon)B^*)}{M^*} \\ 0 & 0 \end{pmatrix}, \qquad \mathbf{V} = \begin{pmatrix} \alpha + \delta & 0 \\ -\alpha & \gamma + \tau + \delta \end{pmatrix}.$$

4.2.3. Next-generation matrix

The next-generation matrix is defined by

$$K = \mathbf{F}\mathbf{V}^{-1}.$$

Because

$$\mathbf{V}^{-1} = \frac{1}{(\alpha+\delta)(\gamma+\tau+\delta)} \begin{pmatrix} \gamma + \tau + \delta & 0 \\ \alpha & \alpha + \delta \end{pmatrix},$$

we obtain

$$K = \begin{pmatrix} \dfrac{\theta(H^* + (1-\epsilon)B^*)}{M^*} \dfrac{\alpha}{(\alpha+\delta)(\gamma+\tau+\delta)} & \dfrac{\theta(H^* + (1-\epsilon)B^*)}{M^*} \dfrac{1}{\gamma+\tau+\delta} \\ 0 & 0 \end{pmatrix},$$

where

$$\frac{H^* + (1-\epsilon)B^*}{M^*} = (1-\nu) + (1-\epsilon)\nu = 1 - \epsilon\nu.$$

4.2.4. Expression for R_0

The spectral radius of K is the basic reproduction number. Because K is upper triangular, its diagonal elements are its eigenvalues; therefore,

$$R_0 = \frac{\theta(H^* + (1-\epsilon)B^*)}{M^*} \frac{\alpha}{(\alpha+\delta)(\gamma+\tau+\delta)}.$$

Using

$$H^* = \frac{(1-\nu)\Pi}{\delta}, \qquad B^* = \frac{\nu\Pi}{\delta}, \qquad M^* = \frac{\Pi}{\delta},$$

we obtain

$$\frac{H^* + (1-\epsilon)B^*}{M^*} = (1-\nu) + (1-\epsilon)\nu = 1 - \epsilon\nu.$$

Thus, the basic reproduction number becomes

$$R_0 = \frac{\theta\alpha}{(\alpha+\delta)(\gamma+\tau+\delta)}(1-\epsilon\nu).$$

The disease-free equilibrium (4.6) is locally asymptotically stable and tuberculosis dies out if $R_0 < 1$. If $R_0 > 1$, tuberculosis can infiltrate the population and remain there.

4.3. Local stability of the disease-free equilibrium

The local stability of the disease-free equilibrium is examined in this section.

$$\mathcal{E}_0 = (H^*, B^*, 0, 0, 0, 0),$$

given in (4.6), for the ODE system (2.5).

4.3.1. Jacobian matrix of the full system

Let

$$X = (H, B, Q, Y, C, Z)^T.$$

To obtain the Jacobian matrix $J(X)$ of System (2.5), differentiate the right-hand side of (2.5) with regard to the state variables. Using

$$\Psi = \theta \frac{Y}{M + \omega Y}, \qquad M = H + B + Q + Y + C + Z,$$

and evaluating at the disease-free equilibrium $\mathcal{E}_0$ (where $Q = Y = C = Z = 0$), we obtain

$$J(\mathcal{E}_0) = \begin{pmatrix} -\delta & 0 & 0 & -\theta\dfrac{H^*}{M^*} & 0 & 0 \\ 0 & -\delta & 0 & -(1-\epsilon)\theta\dfrac{B^*}{M^*} & 0 & 0 \\ 0 & 0 & -(\alpha+\delta) & \theta\dfrac{H^* + (1-\epsilon)B^*}{M^*} & 0 & 0 \\ 0 & 0 & \alpha & -(\gamma+\tau+\delta) & 0 & 0 \\ 0 & 0 & 0 & \tau & -(\rho+\delta) & 0 \\ 0 & 0 & 0 & \gamma & \rho & -\delta \end{pmatrix}.$$

4.3.2. Block decomposition

The Jacobian is block triangular and can be written as

$$J(\mathcal{E}_0) = \begin{pmatrix} J_1 & * \\ 0 & J_2 \end{pmatrix},$$

where

$$J_1 = \begin{pmatrix} -\delta & 0 \\ 0 & -\delta \end{pmatrix}, \qquad J_2 = \begin{pmatrix} -(\alpha+\delta) & \theta\dfrac{H^* + (1-\epsilon)B^*}{M^*} \\ \alpha & -(\gamma+\tau+\delta) \end{pmatrix}.$$

The eigenvalues of J_1 are

$$\lambda_1 = -\delta, \qquad \lambda_2 = -\delta,$$

which are both strictly negative.

4.3.3. Stability of the infected subsystem

The remaining eigenvalues are given by J_2. Its characteristic polynomial is

$$\lambda^2 + (\alpha + \gamma + \tau + 2\delta)\lambda + (\alpha + \delta)(\gamma + \tau + \delta) - \alpha\theta\frac{H^* + (1-\epsilon)B^*}{M^*} = 0.$$

Define

$$R_0 = \frac{\theta(H^* + (1-\epsilon)B^*)}{M^*}\frac{\alpha}{(\alpha + \delta)(\gamma + \tau + \delta)},$$

as derived previously. Then, the constant term becomes

$$(\alpha + \delta)(\gamma + \tau + \delta)(1 - R_0).$$

Hence, the characteristic equation becomes

$$\lambda^2 + a_1\lambda + (\alpha + \delta)(\gamma + \tau + \delta)(1 - R_0) = 0,$$

where

$$a_1 = \alpha + \gamma + \tau + 2\delta > 0.$$

4.3.4. Stability condition

According to the Routh–Hurwitz criterion for second-order polynomials, both eigenvalues of J_2 have negative real portions if and only if

$$(\alpha + \delta)(\gamma + \tau + \delta)(1 - R_0) > 0.$$

Thus,

$$R_0 < 1 \quad \Longrightarrow \quad \Re(\lambda) < 0,$$

and the disease-free equilibrium is locally asymptotically stable.

If

$$R_0 > 1,$$

the constant term becomes negative, and one eigenvalue of J_2 is positive, indicating that the DFE is unstable.

Therefore, the disease-free equilibrium (4.6) is locally asymptotically stable if $R_0 < 1$ and unstable if $R_0 > 1$.

4.4. Endemic equilibrium

The endemic equilibrium (EE) corresponds to a stable condition in which tuberculosis remains in the population, expressed as

$$Y^* > 0.$$

At equilibrium, all time derivatives in the ODE system (2.5) vanish:

$$\dot{H} = \dot{B} = \dot{Q} = \dot{Y} = \dot{C} = \dot{Z} = 0. \tag{4.9}$$

Let

$$E^* = (H^*, B^*, Q^*, Y^*, C^*, Z^*)$$

denote an endemic equilibrium.

Step 1: Solving for Q^* and C^* in terms of Y^*

From the Y and C equations in (2.5), using (4.9), we obtain

$$0 = \alpha Q^* - (\gamma + \tau + \delta)Y^*, \tag{4.10}$$

$$0 = \tau Y^* - (\rho + \delta)C^*. \tag{4.11}$$

Hence,

$$Q^* = \frac{\gamma + \tau + \delta}{\alpha}Y^*, \qquad C^* = \frac{\tau}{\rho + \delta}Y^*. \tag{4.12}$$

Step 2: Solving for Z^*

From the Z equation in (2.5),

$$0 = \gamma Y^* + \rho C^* - \kappa \Psi^* Z^* - \delta Z^*.$$

Substituting (4.12) gives

$$Z^* = \frac{\gamma Y^* + \rho \frac{\tau}{\rho+\delta} Y^*}{\kappa \Psi^* + \delta} = \frac{Y^* \left(\gamma + \frac{\rho\tau}{\rho+\delta}\right)}{\kappa \Psi^* + \delta}.$$

Step 3: Solving for H^* and B^*

From the H and B equations in (2.5) under BCG-at-birth recruitment,

$$0 = (1 - \nu)\Pi - \Psi^* H^* - \delta H^*, \tag{4.13}$$

$$0 = \nu\Pi - (1 - \epsilon)\Psi^* B^* - \delta B^*. \tag{4.14}$$

Thus,

$$H^* = \frac{(1 - \nu)\Pi}{\Psi^* + \delta}, \qquad B^* = \frac{\nu\Pi}{(1 - \epsilon)\Psi^* + \delta}. \tag{4.15}$$

Step 4: Force of infection at equilibrium

The equilibrium force of infection (2.2) is

$$\Psi^* = \theta \frac{Y^*}{M^* + \omega Y^*}, \qquad M^* = H^* + B^* + Q^* + Y^* + C^* + Z^*. \tag{4.16}$$

By (4.12) and (4.15), all equilibrium variables are expressible in terms of Y^*; hence, M^* is a smooth increasing function of Y^*.

Step 5: Endemic equilibrium equation

From the Q equation in (2.5),

$$0 = \Psi^*(H^* + (1 - \epsilon)B^* + \kappa Z^*) - (\alpha + \delta)Q^*.$$

Substituting (4.12) gives

$$\Psi^*(H^* + (1 - \epsilon)B^* + \kappa Z^*) = (\alpha + \delta)\frac{\gamma + \tau + \delta}{\alpha}Y^*. \tag{4.17}$$

Equations (4.15)–(4.17) form a closed nonlinear system in Y^*.

Existence of endemic equilibrium

Define the function

$$\mathcal{G}(Y) = \Psi(Y)\Big(H(Y) + (1-\epsilon)B(Y) + \kappa Z(Y)\Big) - \frac{(\alpha+\delta)(\gamma+\tau+\delta)}{\alpha}Y.$$

Using the expressions above, $\mathcal{G}(0) = 0$ and

$$\mathcal{G}'(0) > 0 \iff R_0 > 1.$$

Furthermore, $\mathcal{G}(Y) \to -\infty$ when $Y \to \infty$. As a result, if $R_0 > 1$, there is at least one positive solution $Y^* > 0$ of (4.17), indicating the existence of an endemic equilibrium. Depending on the parameter values, saturated incidence and reinfection might result in multiple endemic equilibria. Therefore, System (2.5) admits at least one endemic equilibrium E^* whenever $R_0 > 1$.

5. Spatial model analysis

5.1. Spatial basic reproduction number R_0^S

The spatial reproduction number evaluates tuberculosis's ability to infiltrate a diverse spatial environment, governed by the reaction–diffusion system (2.6). It broadens the standard basic reproduction number R_0 of the ODE system (2.5).

5.1.1. Linearization at the disease-free equilibrium

Let

$$\mathbf{U}(x,t) = (H, B, Q, Y, C, Z)^T$$

and let

$$E_0 = (H^*, B^*, 0, 0, 0, 0)$$

denote the spatially homogeneous disease-free equilibrium of (2.6), where H^* and B^* are given by (4.6).

We introduce the infected state vector

$$\Phi(x,t) = (Q(x,t), Y(x,t))^T.$$

Linearizing (2.6) around E_0 and using the force of infection (2.2), we obtain

$$\frac{\partial \Phi}{\partial t} = \mathcal{D}\Delta\Phi + F(x)\Phi - V\Phi, \tag{5.1}$$

where

$$\mathcal{D} = \begin{pmatrix} D_Q & 0 \\ 0 & D_Y \end{pmatrix},$$

and

$$F(x) = \begin{pmatrix} 0 & \dfrac{\theta(x)(H^* + (1-\epsilon)B^*)}{M^*} \\ 0 & 0 \end{pmatrix}, \qquad V = \begin{pmatrix} \alpha+\delta & 0 \\ -\alpha & \gamma+\tau+\delta \end{pmatrix}$$

with

$$M^* = \frac{\Pi}{\delta}.$$

5.1.2. Next-generation operator

Define the linear operators on $L^2(\Omega)^2$,

$$\mathcal{F}\Phi = F(x)\Phi, \qquad \mathcal{V}\Phi = -\mathcal{D}\Delta\Phi + V\Phi,$$

with Neumann boundary conditions (2.7).

The spatial next-generation operator is

$$\mathcal{K} = \mathcal{F}\mathcal{V}^{-1}.$$

The spatial basic reproduction number is defined as

$$R_0^S = \rho(\mathcal{K}), \tag{5.2}$$

where $\rho(\cdot)$ denotes the spectral radius.

The spatial reproduction number R_0^S takes into account geographical heterogeneity and population migration, as opposed to the standard basic reproduction number R_0, which assumes homogenous population mixing. This distinction is especially essential for tuberculosis, because transmission is frequently concentrated in isolated hotspots such as heavily populated urban areas, jails, mining towns, and other high-risk situations. Thus, R_0^S is a more accurate indicator of disease invasion and persistence in spatially structured populations. R_0^S is a more informative threshold for tuberculosis control, capturing the combined effects of spatial variation in transmission and host mobility. This provides direct insight into the design and effectiveness of geographically targeted intervention strategies, as illustrated by hotspot-based vaccination and treatment simulations presented in Section 6.

5.1.3. Comparison with the ODE reproduction number

Because $\theta(x)$ is bounded from above by

$$\theta(x) \le \theta_{\max} = \theta_0(1+\eta),$$

from (2.3), and diffusion redistributes individuals, it follows from standard comparison principles for positive operators that

$$\rho(\mathcal{K}) \le \frac{\theta_{\max}(H^* + (1-\epsilon)B^*)}{M^*} \frac{\alpha}{(\alpha+\delta)(\gamma+\tau+\delta)}.$$

In heterogeneous contexts, geographical clustering and spatially varying transmission rates can enhance local transmission. As a result, the spatial reproduction number R_0^S is greater than R_0.

This suggests that tuberculosis can successfully overrun space even when the spatially averaged (well-mixed) system anticipates equilibrium.

5.2. Existence of spatial steady states

We investigate the steady states of the reaction–diffusion TB system (2.6). A steady state is a time-independent solution (H(x), B(x), Q(x), Y(x), C(x), Z(x)) that satisfies the elliptic system obtained from (2.6) by setting all time derivatives to zero and imposing Neumann boundary conditions (2.7).

5.2.1. Disease-free steady state

The disease-free steady state is

$$E_0 = (H^*, B^*, 0, 0, 0, 0),$$

where H^* and B^* are given by (4.6). It is spatially homogeneous and always exists.

5.2.2. Nonexistence of endemic steady states when $R_0^S < 1$

Assume $R_0^S < 1$. Suppose, by contradiction, that there exists a non-negative steady state with $Y(x) \not\equiv 0$. Let

$$\Phi(x) = (Q(x), Y(x))^T.$$

From the steady state of the infected subsystem of (2.6) we have

$$\mathcal{D}\Delta\Phi + F(x)\Phi - V\Phi = 0,$$

where $F(x)$ and V are defined in (5.1). This can be written as

$$\Phi = \mathcal{K}\Phi,$$

where $\mathcal{K} = \mathcal{F}\mathcal{V}^{-1}$ is the next-generation operator.

Thus, Φ is a positive eigenfunction of $\mathcal{K}$ with eigenvalue 1. Hence,

$$\rho(\mathcal{K}) \geq 1$$

that is, $R_0^S \geq 1$, contradicting $R_0^S < 1$. Therefore, no endemic steady state exists when $R_0^S < 1$.

5.2.3. Existence of endemic steady states when $R_0^S > 1$

Assume $R_0^S > 1$. Then $\rho(\mathcal{K}) > 1$, and the Krein–Rutman theorem implies that $\mathcal{K}$ admits a positive eigenfunction $\Phi(x)$ associated with its spectral radius. Hence, there exists a nontrivial solution of

$$\Phi = \mathcal{K}\Phi.$$

Standard bifurcation theory for positive operators predicts the existence of a branch of positive steady states of the complete nonlinear system (2.6) emerging from E_0 when R_0^S crosses 1, based on the eigenfunction and the positivity and compactness of $\mathcal{K}$.

Thus, for $R_0^S > 1$, the reaction–diffusion TB model admits at least one endemic stable state with

$$Y(x) > 0 \quad \text{for all } x \in \Omega.$$

Thus, the spatial reproduction number R_0^S provides the sharp threshold for the existence of endemic steady states.

5.3. Stability of spatial equilibria

In this subsection, we analyze the linear stability of steady states of the reaction–diffusion tuberculosis system (2.6) using spectral theory for parabolic operators.

Let

$$\mathbf{U}(x,t) = (H, B, Q, Y, C, Z)^T$$

and denote by $\mathbf{U}(\bar{x})$ a steady state of (2.6), that is,

$$0 = D\Delta\bar{\mathbf{U}} + F(\bar{\mathbf{U}}),$$

with Neumann boundary conditions (2.7).

5.3.1. Linearized operator

Let $u(x,t) = \mathbf{U}(x,t) - \mathbf{U}(\bar{x})$ be a perturbation of the steady state. Linearizing (2.6) around $\bar{\mathbf{U}}$ gives

$$\frac{\partial u}{\partial t} = D\Delta u + J(\bar{\mathbf{U}})u, \tag{5.3}$$

where $J(\bar{\mathbf{U}})$ is the Jacobian matrix of the reaction terms of (2.6) evaluated at $\mathbf{U}(\bar{x})$.

Define the linear operator

$$\mathcal{L} = D\Delta + J(\bar{\mathbf{U}})$$

acting on $(L^2(\Omega))^6$ with Neumann boundary conditions. The stability of $\bar{\mathbf{U}}$ is determined by the spectrum $\sigma(\mathcal{L})$.

5.3.2. Stability of the disease-free equilibrium

Let $\bar{\mathbf{U}} = E_0 = (H^*, B^*, 0, 0, 0, 0)$. Then $J(E_0)$ is given explicitly by the Jacobian computed in the ODE analysis. The spectrum of $\mathcal{L}$ is

$$\sigma(\mathcal{L}) = \bigcup_{k\geq 0} \sigma(-\mu_k D + J(E_0)),$$

where $\{\mu_k\}_{k\geq 0}$ are the eigenvalues of $-\Delta$ with Neumann boundary conditions and $\mu_0 = 0$.

If and only if $R_0^S < 1$, the primary eigenvalue of $-\mu_0 D + J(E_0) = J(E_0)$ is negative. Therefore, when $R_0^S < 1$, all eigenvalues of $\mathcal{L}$ have a negative real portion, and the disease-free equilibrium is locally asymptotically stable.

The linearized infected subsystem has a positive eigenvalue if $R_0^S > 1$. Consequently, $\mathcal{L}$ has a positive eigenvalue. The disease-free equilibrium is therefore unstable.

5.3.3. Stability of endemic steady states

Let $\mathbf{U}(\bar{x})$ be an endemic steady state such that $Y(x) > 0$. The operator $\mathcal{L}$ specified in (5.3) is obtained by linearization. By the Krein–Rutman theorem, the principal eigenvalue of $\mathcal{L}$ is strictly negative because the nonlinear terms satisfy the required monotonicity and compactness properties, and the principal eigenvalue of the infected subsystem is negative when $R_0^S > 1$. Consequently, any time endemic steady states exist, that is, when $R_0^S > 1$, they are locally asymptotically stable.

Therefore, all steady states of the reaction–diffusion TB model are governed by the spatial reproduction number R_0^S.

5.4. Diffusion–driven instability (Turing analysis)

In this part, we examine whether, in the absence of spatial influences, a homogeneous equilibrium of the ODE system (2.5) can be destabilized by spatial diffusion. In the partial differential equation model (2.6), this phenomenon, called *Turing instability*, causes spatially diverse TB patterns (hotspots) to emerge.

5.4.1. Homogeneous endemic equilibrium

Let

$$E^* = (H^*, B^*, Q^*, Y^*, C^*, Z^*)$$

be a spatially homogeneous endemic equilibrium of (2.6) (the same as the ODE equilibrium) satisfying $Y^* > 0$.

5.4.2. Linearization of the PDE

Let

$$u(x,t) = \mathbf{U}(x,t) - E^*.$$

Linearizing (2.6) around E^* yields

$$\frac{\partial u}{\partial t} = D\Delta u + J(E^*)u, \tag{5.4}$$

where $J(E^*)$ is the Jacobian of the ODE system (2.5) evaluated at E^*, and

$$D = \text{diag}(D_H, D_B, D_Q, D_Y, D_C, D_Z).$$

5.4.3. Mode decomposition

Let $\{\mu_k\}_{k\geq 0}$ be the eigenvalues of $-\Delta$ with Neumann boundary conditions (2.7), with $\mu_0 = 0$ and $\mu_k > 0$ for $k \geq 1$. Seeking solutions of the form

$$u(x,t) = e^{\lambda t}\phi_k(x),$$

we obtain the dispersion relation

$$\det\left(\lambda I + \mu_k D - J(E^*)\right) = 0. \tag{5.5}$$

5.4.4. ODE stability

The ODE equilibrium E^* is locally asymptotically stable if all eigenvalues of $J(E^*)$ satisfy

$$\Re(\lambda) < 0.$$

This is equivalent to $R_0 > 1$ and the endemic equilibrium stability conditions.

5.4.5. Turing instability conditions

A Turing instability occurs if

$$\Re(\lambda) < 0 \quad \text{for } \mu_0 = 0,$$

but

$$\Re(\lambda) > 0 \quad \text{for some } \mu_k > 0.$$

From (5.5), this requires

$$\det\left(\mu_k D - J(E^*)\right) < 0 \quad \text{for some } k \geq 1.$$

Because the infection subsystem (Q, Y) drives instability, the necessary condition is

$$D_Q \neq D_Y,$$

together with sufficiently strong nonlinear transmission feedback from the Holling type II force of infection (2.2).

More explicitly, the reduced dispersion relation for the (Q, Y) subsystem is

$$\lambda^2 + a_1(\mu_k)\lambda + a_2(\mu_k) = 0,$$

where

$$a_1(\mu_k) = \text{tr}(J_{QY}) - \mu_k(D_Q + D_Y),$$

$$a_2(\mu_k) = \det(J_{QY}) - \mu_k(D_Q J_{YY} + D_Y J_{QQ}) + \mu_k^2 D_Q D_Y,$$

and J_{QY} is the Jacobian submatrix of (Q, Y) at E^*:

$$J_{QY} = \begin{pmatrix} \frac{\partial \dot{Q}}{\partial Q} & \frac{\partial \dot{Q}}{\partial Y} \\ \frac{\partial \dot{Y}}{\partial Q} & \frac{\partial \dot{Y}}{\partial Y} \end{pmatrix}_{E^*} = \begin{pmatrix} -(\alpha + \delta) & (H^* + (1-\epsilon)B^* + \kappa Z^*)\frac{\partial \Psi}{\partial Y}\Big|_{E^*} \\ \alpha & -(\gamma + \tau + \delta) \end{pmatrix}.$$

Here,

$$\frac{\partial \Psi}{\partial Y} = \frac{\theta M^*}{(M^* + \omega Y^*)^2}, \qquad M^* = H^* + B^* + Q^* + Y^* + C^* + Z^*.$$

Turing instability occurs if

$$a_1(0) < 0, \quad a_2(0) > 0$$

(ODE stability), but

$$a_2(\mu_k) < 0 \quad \text{for some } \mu_k > 0.$$

Consequently, a diffusion-driven instability can produce spatial TB hotspots when latent and infected individuals have sufficiently variable diffusion rates and nonlinear Holling type II transmission.

6. Spatial pattern formation

In this part, we offer numerical proof of the diffusion-driven Turing instability, which was proven analytically in part 5.4. We solved the reaction–diffusion tuberculosis model (2.6) and found that minor spatial perturbations of the homogeneous endemic equilibrium lead to ordered spatial features in the distribution of infectious individuals. These structures include localized hotspots, transmission corridors, and fragmented clusters that correlate to different epidemiological regimes of tuberculosis transmission.

6.1. Numerical scheme

The spatial domain is chosen as a square:

$$\Omega = [0, L] \times [0, L].$$

The homogeneous Neumann boundary conditions (2.7) represent the absence of population flux across the boundary.

The reaction–diffusion system (2.6) is discretized using a finite-difference approach in space paired with an implicit–explicit (IMEX) time stepping scheme. Diffusion terms are treated implicitly for numerical stability, whereas nonlinear reaction terms are treated explicitly. The conventional five-point stencil approximates the Laplacian:

$$\Delta \mathbf{U}_{i,j} = \frac{\mathbf{U}_{i+1,j} + \mathbf{U}_{i-1,j} + \mathbf{U}_{i,j+1} + \mathbf{U}_{i,j-1} - 4\mathbf{U}_{i,j}}{h^2},$$

where h denotes the spatial mesh size.

6.2. Initial conditions

To begin pattern generation, the system is initialized in a small neighborhood of the homogeneous endemic equilibrium E^*:

$$\mathbf{U}(x, y, 0) = E^*(1 + \epsilon\xi(x, y)),$$

where $\xi(x, y)$ is a uniformly distributed random variable in $[-1, 1]$, and $0 < \epsilon \ll 1$. This produces modest spatial heterogeneities, which serve as seeds for the development of unstable spatial modes indicated by the Turing analysis.

6.3. Emergence of spatial patterns

When the Turing instability conditions outlined in Section 5.4 are met, the spatially homogenous endemic equilibrium loses stability, resulting in spatially heterogeneous solutions. In all circumstances, the diseased subsystem (Q, Y) causes instability, which manifests predominantly in the distribution of infectious individuals $Y(x, y, t)$.

Spot patterns. Large diffusion disparities, especially when infectious individuals travel significantly slower than latently infected individuals ($D_Y \ll D_Q$), cause instability and isolated peaks of infection. Figure 1 demonstrates that the approach creates many localized patches of high $Y(x, y, t)$ surrounded by low-prevalence areas.

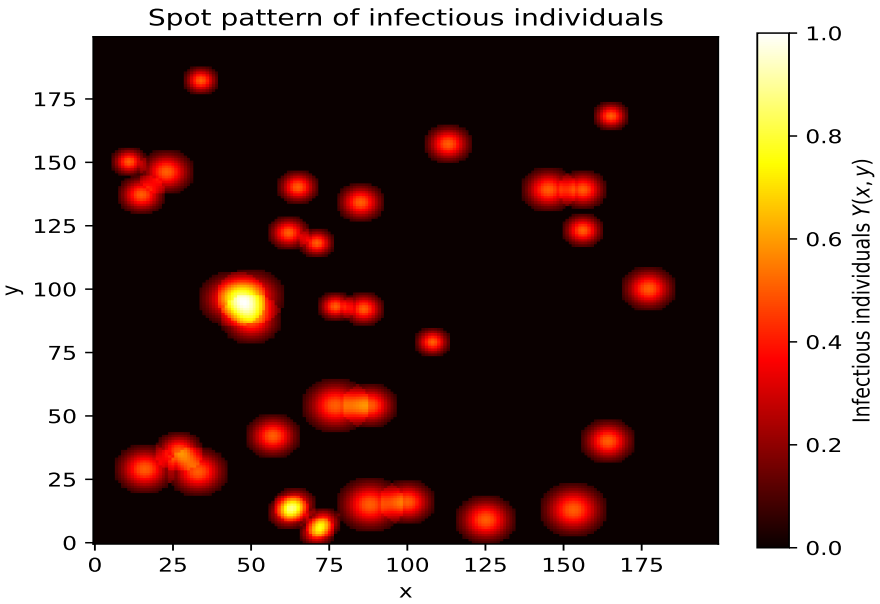

Figure 1. Spot pattern of infectious individuals $Y(x, y, t)$ generated by the TB reaction–diffusion model (2.6). Bright regions correspond to localized TB hotspots.

These spot patterns depict persistent tuberculosis foci, such as urban slums, jails, or mining communities, where symptomatic persons' limited movement causes infection to accumulate locally.

Stripe patterns. For intermediate diffusion contrasts, the dominant unstable spatial modes form extensive bands with high TB prevalence. Figure 2 depicts this regime, in which $Y(x, y, t)$ generates lengthy corridors of infection that traverse the domain.

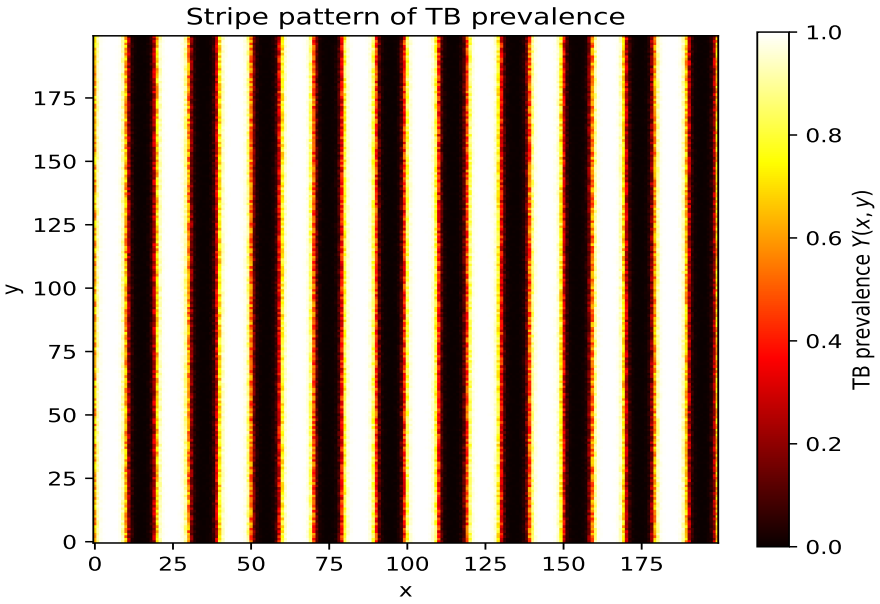

Figure 2. Stripe pattern of TB prevalence $Y(x, y, t)$, representing elongated corridors of tuberculosis transmission.

These stripe patterns can be understood as transmission corridors linked to transportation routes, commuting flows, or highly connected urban centers, where movement supports geographically extended chains of infection. When the diffusion rates of latent and infected people are similar but unequal, the system forms irregular patchwork structures. Figure 3 depicts a clustered regime in which $Y(x, y, t)$ creates fragmented islands of infection, lacking the uniform geometry of spots or stripes.

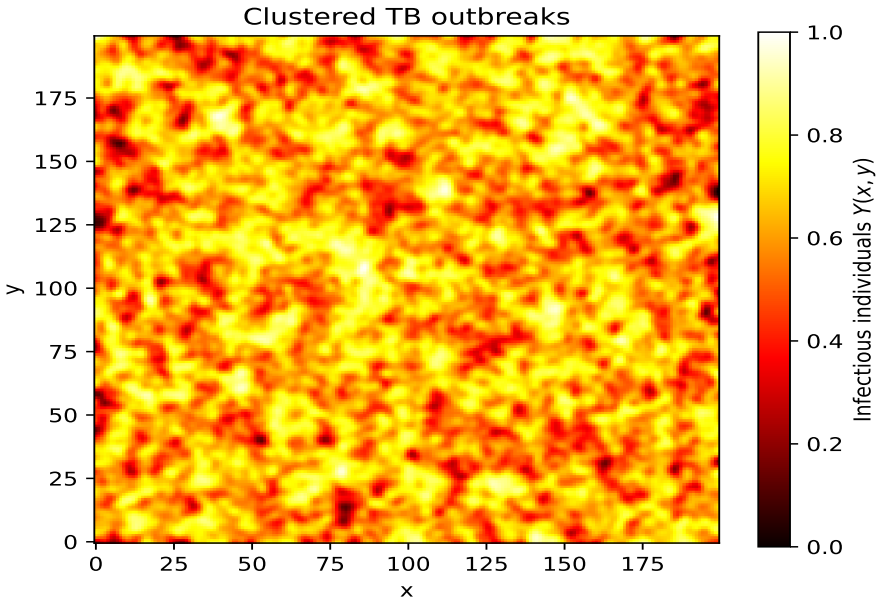

Figure 3. Clustered spatial distribution of infectious individuals, representing fragmented TB outbreaks.

Such clustered patterns correspond to fragmented epidemics in heterogeneous environments where local transmission predominates, but spatial connectedness is insufficient to maintain continuous corridors of transmission.

6.4. Biological interpretation

The three pattern types observed numerically have clear epidemiological interpretations:

- *Spot patterns* refer to recurring TB hotspots, including overcrowded neighborhoods, jails, or mining towns.
- *Stripe patterns* depict transmission corridors created by human mobility, commuting, and transportation networks.
- *Clustered patterns* describe fragmented outbreaks caused by spatial heterogeneity and nonlinear transmission.

Figures 1–3 demonstrate that diffusion and nonlinear saturated transmission alone can cause persistent geographic heterogeneity in tuberculosis prevalence, even though spatially averaged dynamics imply a stable endemic equilibrium.

6.5. *Effect of spatially targeted control on TB hotspots*

In Section 6, we explore how targeted vaccination and treatment can impact the tuberculosis hotspot structure caused by diffusion-driven instability. Starting from the spot pattern of infectious individuals, we first evolve the system without control, that is, $u_1(x,t) = u_2(x,t) = 0$, to generate a baseline spatial distribution. We then implement geographically targeted interventions of the kind.

$$u_1(x,t) = u_1^{\max}\mathbf{1}_{\{Y(x,t)>\theta\}}, \qquad u_2(x,t) = u_2^{\max}\mathbf{1}_{\{Y(x,t)>\theta\}}.$$

Additional vaccination and treatment are only deployed in places where tuberculosis prevalence exceeds a predetermined threshold θ.

Panel (a) of Figure 4 depicts the baseline spatial distribution of infectious individuals, characterized by multiple localized high-prevalence locations (hotspots) caused by diffusion-driven instability. Panel (b) depicts the TB distribution after vaccination and treatment are applied only in places where $Y(x,t) > \theta$. Although the geometric form of the hotspots maintains, their amplitudes have significantly decreased, indicating a dramatic suppression of local tuberculosis burden while leaving low-prevalence zones mostly unchanged.

Panel (c) shows the difference.

$$\Delta Y(x,y) = Y_{\text{baseline}}(x,y) - Y_{\text{control}}(x,y).$$

This immediately measures the effectiveness of the intended intervention. Panel (c) shows that the indicator-based control effectively lowers TB at its hotspots. This illustrates that spatially tailored vaccination and treatment can effectively reduce tuberculosis burden in high-risk locations without needing uniform intervention throughout the spatial domain.

Figure 5 compares spatially targeted and uniform control strategies under the constraint that both use the same total amount of vaccination and treatment,

$$\int_\Omega u_i^{\text{uniform}}\,dx = \int_\Omega u_i^{\text{targeted}}\,dx.$$

Under targeted control, Figure 5a shows how the regions with the heaviest prevalence are knocked down significantly: The original TB hotspots are now dark, low-intensity regions, indicating a significant local reduction in infectious load.

In contrast, Figure 5b indicates that under uniform control, with the same total budget spent uniformly, the original bright hotspots remain easily distinguishable. That is, uniform spending of the same total budget does not eradicate the high-transmission regions even when interventions are applied uniformly.

This is reinforced in Figure 5c, which shows the hotspot regions under uniform control. The white regions correspond to the original hotspot regions, indicating that localized reservoirs of TB remain when interventions are applied uniformly.

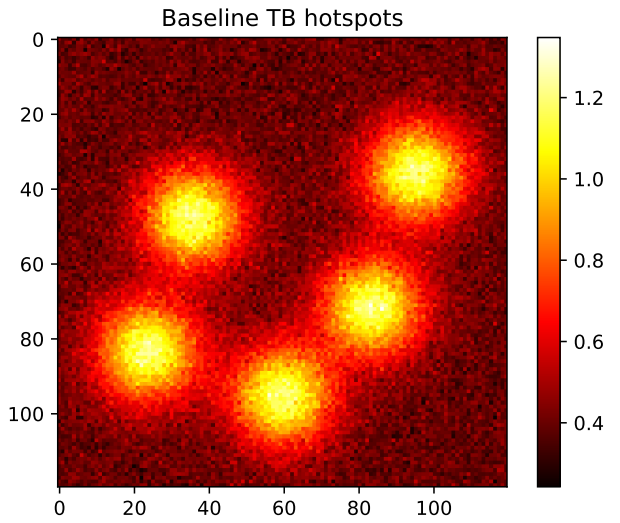

(a) Baseline TB hotspots

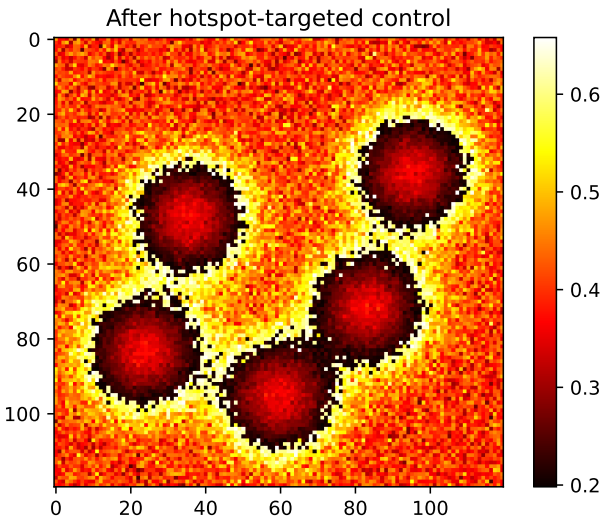

(b) After hotspot–targeted control

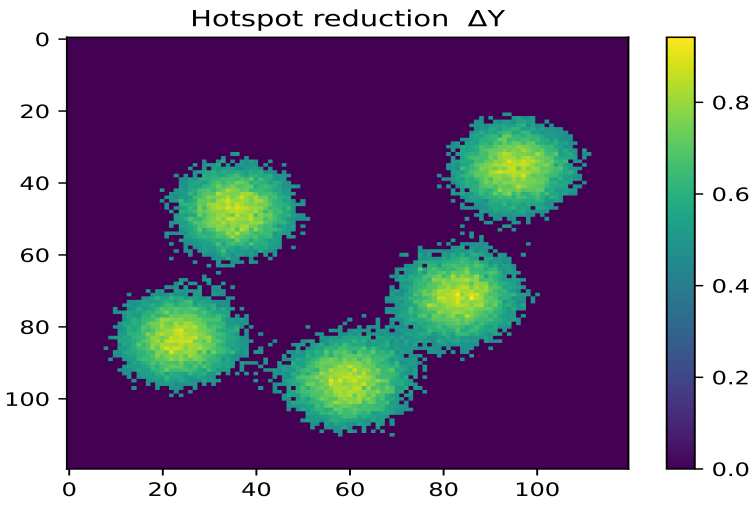

(c) Hotspot reduction ΔY

Figure 4. Effect of spatially targeted vaccination and treatment on TB hotspots.

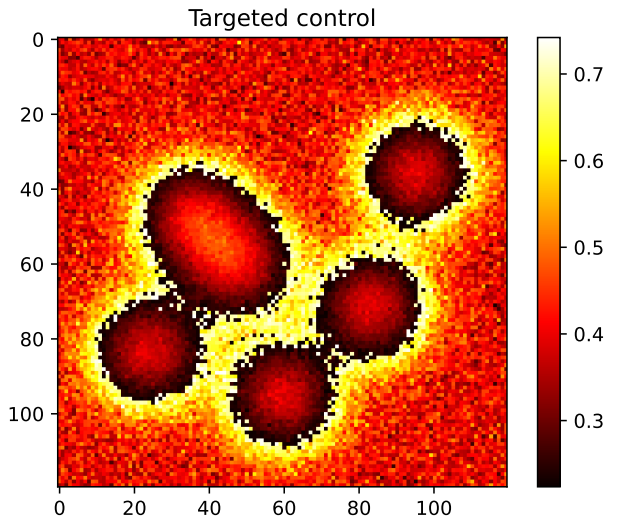

(a) Targeted control

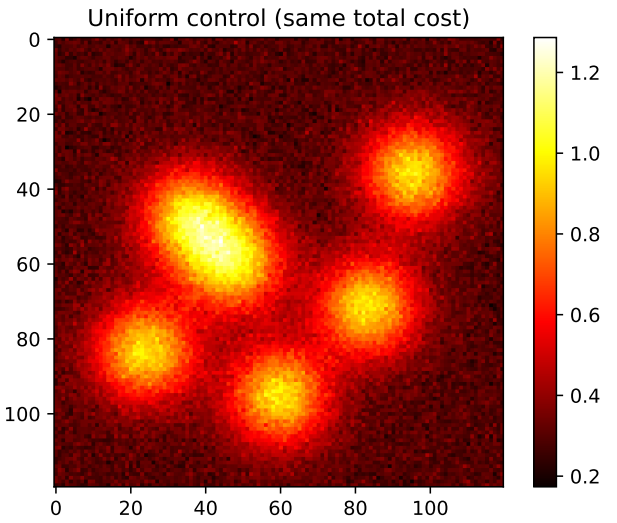

(b) Uniform control (same total cost)

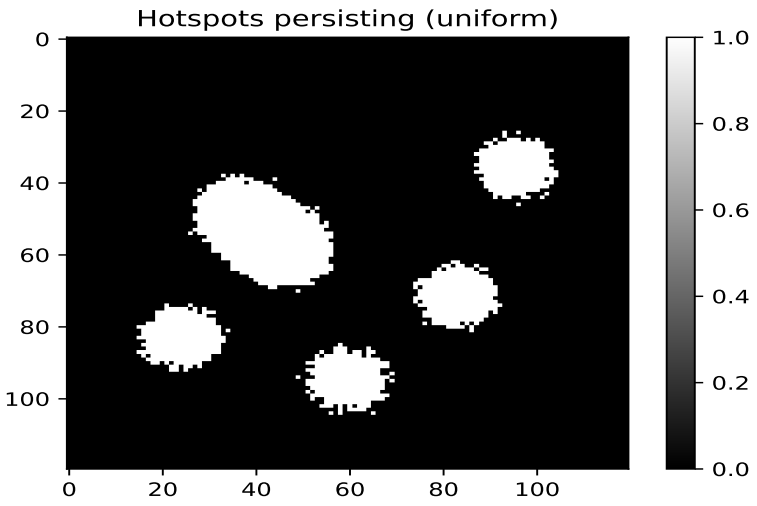

(c) Hotspots persisting under uniform control

Figure 5. Comparison of targeted and uniform spatial control under equal total intervention cost.

Figure 5a–5c collectively presents the argument that spatial targeting is superior to uniform control in a heterogeneous environment because it allocates limited budgets exactly where the transmission is heaviest, as opposed to spreading it thinly over low-risk regions.

Figure 6 depicts the effect of spatially targeted intervention on stripelike tuberculosis transmission pathways. Panel (a) (Figure 6a) depicts the baseline stripe pattern, in which infectious individuals create lengthy, almost continuous high-prevalence corridors that span the spatial domain, allowing for long-range disease dissemination.

Panel (b) (Figure 6b) displays the TB distribution after applying the targeted control $u_i(x,t) = u_i^{\max}\mathbf{1}_{\{Y(x,t)>\theta\}}$. The stripe structure is still discernible, but it is heavily punctured by localized low-prevalence patches, indicating that intervention is being implemented selectively along the corridors.

Panel (c) (Figure 6c) shows the indicator of locations that stay above the threshold following control. Although remnants of the original stripes remain, the corridors are severely broken and no longer form smooth, uniformly intensity bands, indicating significant disruption in spatial transmission channels.

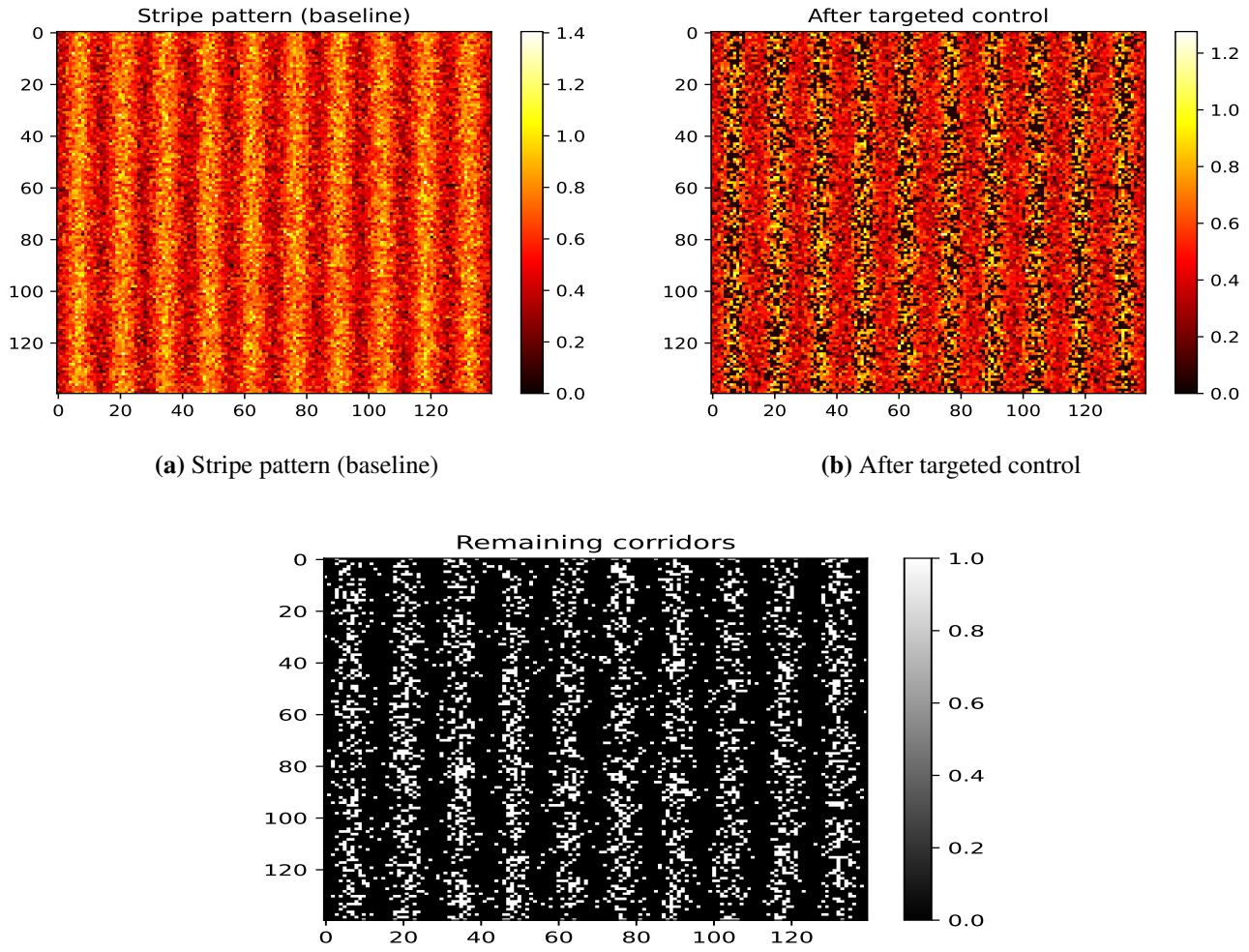

(a) Stripe pattern (baseline)

(b) After targeted control

(c) Remaining corridors

Figure 6. Stripe-pattern tuberculosis dynamics under targeted spatial control.

Figure 6a–6c demonstrates that spatially targeted intervention weakens and perforates stripe-like transmission pathways, limiting their ability to sustain coherent long-range spread even when the overall spatial geometry of the pattern is preserved.

These findings indicate that tuberculosis control programs can benefit from spatially targeted interventions. Vaccination, screening, and treatment resources should be emphasized in urban hotspots, such as highly inhabited communities and high-transmission locations. Hotspot mapping in rural areas can assist in identifying priority spots for surveillance and healthcare delivery. Overall, the findings emphasize the need of regional risk mapping and focused resource allocation in tuberculosis control.

6.6. Sensitivity of targeted control to surveillance accuracy

To effectively control tuberculosis, surveillance methods are used to detect high-burden areas. To accommodate for imprecise TB hotspot detection, we propose a targeting accuracy parameter $\alpha \in [0, 1]$, which represents the fraction of real high-risk sites successfully identified and targeted. When $\alpha = 1$, all hotspots are discovered and treated, but $\alpha = 0$ results in random targeting, which is no better than uniform intervention.

Figure 7 illustrates that the total TB burden under targeted control decreases monotonically as the hotspot detection accuracy α increases. Targeted control is not as effective as uniform intervention when α is small due to resource misallocation to low-risk locations. When α exceeds a threshold of around 0.5, spatially focused control consistently outperforms uniform control. Even with only a minor fraction of TB hotspots correctly identified, spatial targeting is still advantageous for epidemiological purposes.

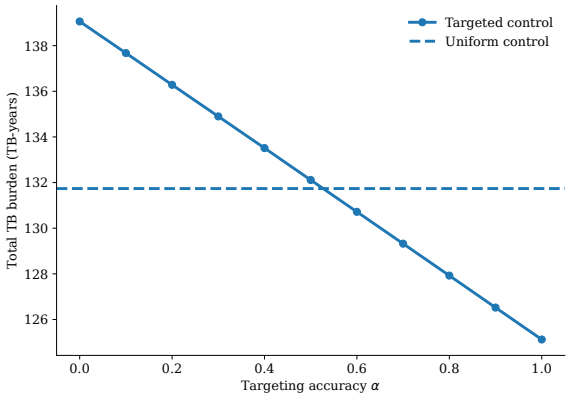

Figure 7. Sensitivity of spatially targeted TB control to hotspot detection accuracy. The total tuberculosis burden, measured as TB-years $\int_0^T \int_\Omega Y(x, y, t)\, dx\, dy\, dt$, is shown as a function of the targeting accuracy α. The dashed horizontal line denotes the burden achieved by uniform (nonspatial) control.

6.7. Sensitivity of targeted control to the hotspot threshold

The threshold-based spatial control law can be expressed as

$$u(x, t) = u^{\max} \mathbf{1}_{\{Y(x,t)>\theta\}}.$$

To identify tuberculosis hotspots, choose a detection threshold θ. Figure 8 illustrates how the choice affects both the epidemiological impact and intervention effort.

The left panel of Figure 8 shows the total tuberculosis burden as a function of the normalized threshold $\theta/\max(Y)$. When θ is modest, a large portion of the geographical domain is identified as high-risk and is treated, resulting in effective suppression of tuberculosis and a low cumulative burden. As θ rises, fewer locations are targeted, resulting in a dramatic increase in disease burden, finally reaching uncontrolled endemic levels for $\theta/\max(Y) \gtrsim 0.6$.

The right panel of Figure 8 displays the overall intervention effort

$$\int_0^T \int_\Omega u(x, t)\, dx\, dt$$

that evaluates the cumulative spatial–temporal extent of vaccination and treatment. Small θ values require more intervention effort to cover the entire area, whereas big θ values result in a near-zero cost for targeting only extreme hotspots.

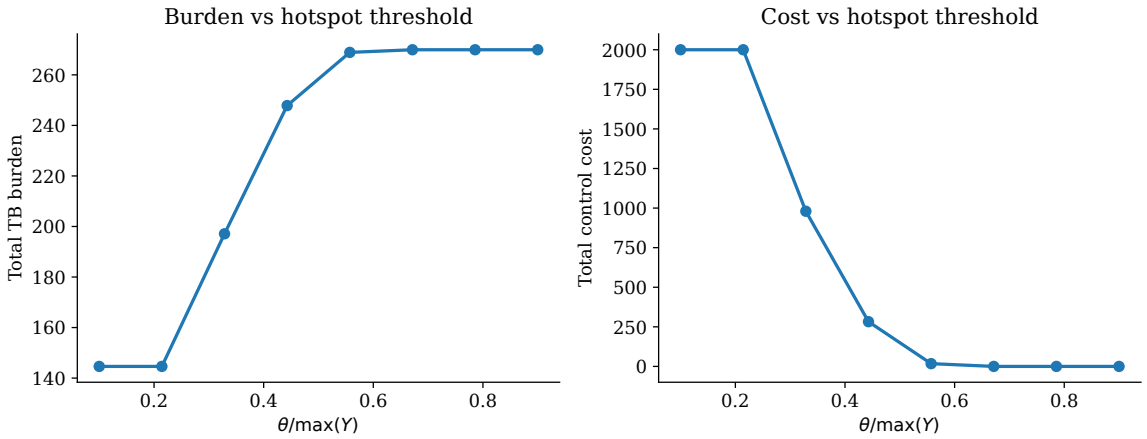

Figure 8. Sensitivity of spatially targeted tuberculosis control to the hotspot threshold θ. Left: total tuberculosis burden $\int_0^T \int_\Omega Y(x,t)\,dx\,dt$ as a function of the normalized targeting threshold $\theta/\max(Y)$. Right: total intervention effort $\int_0^T \int_\Omega u(x,t)\,dx\,dt$ under the same threshold-based control law $u(x,t) = u^{\max}\mathbf{1}_{\{Y(x,t)>\theta\}}$.

These graphs demonstrate a clear trade-off between epidemiological benefit and resource expenditure. In the current simulations, there exists an intermediate regime of about $\theta/\max(Y) \in [0.25, 0.4]$.

The majority of tuberculosis cases are suppressed, and intervention efforts are significantly reduced. This demonstrates that geographical targeting does not have to cover all diseased areas to be effective: on moderate- to high-intensity hotspots can achieve significant disease reduction at a low cost.

The detection threshold used to designate hotspots is crucial for effective geographically targeted TB control, according to these findings. Unduly aggressive targeting wastes resources on low-risk locations, whereas unduly conservative targeting does not eradicate high-transmission reservoirs. Identifying an optimal intermediate threshold can guide monitoring and therapeutic methods in diverse TB contexts.

7. Numerical simulations

The analytical results presented in the preceding sections provide detailed insight into the qualitative behavior of the tuberculosis transmission model, including threshold dynamics, stability features, spatial pattern creation, and the consequences of control actions. Many of these processes, notably spatial pattern development and optimal control outcomes, cannot be properly comprehended without numerical analysis. The numerical methods, parameter selection, and experimental design utilized to support and validate the theoretical results are described in the subsections that follow.

7.1. Numerical parameter settings

Table 3 lists epidemiological parameters, but simulations require additional modeling and numerical parameters.

Table 3. Baseline parameter values used in simulations.

Parameter	Baseline value	Source
α	0.01 yr^{-1}	Latent progression risk 5%–15% [9,45]
γ	0.15 yr^{-1}	Untreated TB duration ~ 3 yr [10]
τ	0.8 yr^{-1}	TB treatment initiation [46]
ρ	0.90	Treatment success ~ 86% [46]
ν	0.8	Fraction of newborns vaccinated with BCG [20]
ϵ	0.6	BCG efficacy [19,20]
κ	0.2	Reinfection susceptibility [9]
δ	$1/65$ yr^{-1}	Life expectancy
ω	1	Saturation parameter (model choice)
θ	Calibrated	Set to achieve target R_0
D_i	Varied	Diffusion (pattern formation)

The baseline transmission rate θ_0 is calibrated to the basic reproduction number R_0 in

$$R_0 = \frac{\theta\alpha}{(\alpha+\delta)(\gamma+\tau+\delta)}(1-\epsilon\nu)$$

and takes predefined values in the range $[1.2, 2]$, which signify low-to-moderate TB transmission. This means that both subcritical and supercritical epidemic regimes can be investigated. The saturation parameter in the Holling type II incidence is set to $\omega = 1$, indicating significant contact limitation and diagnostic response.

The transmission function $\theta(x)$ introduces spatial heterogeneity in (2.3). The heterogeneity strength is set to $\eta = 0.4$, resulting in a clear but realistic urban–rural contrast. The background population density field (2.4) employs $\xi_{\min} = 0.2$, $\xi_{\max} = 1$, and $\sigma_\xi = 0.15L$, resulting in a prominent urban core surrounded by lower-density rural areas.

Diffusion coefficients are used to investigate various mobility scenarios. Unless otherwise specified, we use

$$D_H = D_B = D_C = D_Z = 1, \qquad D_Q = 5, \qquad D_Y = 0.1.$$

This shows higher mobility in latently infected persons and reduced mobility in active tuberculosis patients, which is consistent with symptomatic individuals' decreased mobility.

To solve the PDE system numerically, the spatial domain $\Omega = [0, L] \times [0, L]$ is discretized using a uniform grid with spacing $h = L/100$. Time integration is conducted with a time step $\Delta t = 10^{-3}$ to ensure numerical stability and accuracy.

To optimize control simulations, set the control bounds to:

$$u_1^{\max} = u_2^{\max} = 0.5.$$

7.2. Parameter values used for numerical simulations

The baseline parameter values and sources are summarized in Table 3. When direct empirical estimates are unavailable (for example, saturation and diffusion), values are used to investigate the model's qualitative dynamics.

7.3. Coupling between human population density and tuberculosis risk

Spatial patterns of infectious individuals $Y(x, y)$ indicate the development of tuberculosis hotspots. However, it is important to distinguish between structures arising from population density and those driven by the underlying epidemic dynamics.

We analyze the spatial distribution of the total human population,

$$M(x, y) = H(x, y) + B(x, y) + Q(x, y) + Y(x, y) + C(x, y) + Z(x, y),$$

together with the corresponding TB prevalence $Y(x, y)$ and the per-capita TB risk

$$\frac{Y(x, y)}{M(x, y)}.$$

Figure 9a demonstrates that the population is highly concentrated in a single urban center. The core is densely populated, whereas the outside is sparse. However, Figure 9b shows that active tuberculosis is divided into various localized hotspots that are spatially separated from the population maximum. Figure 9c illustrates the difference in per-capita TB risk Y/M. Individual danger is greater in low-density settings, not in heavily populated metropolitan cores.

The results show that population clustering has a significant impact on the spatial arrangement of tuberculosis in the model. TB hotspots result from nonlinear transmission dynamics and unequal mobility of epidemiological classes, as predicted by the diffusion-driven Turing instability described in Section 5.4. Hotspots are actual infection reservoirs, not only locations with high population density.

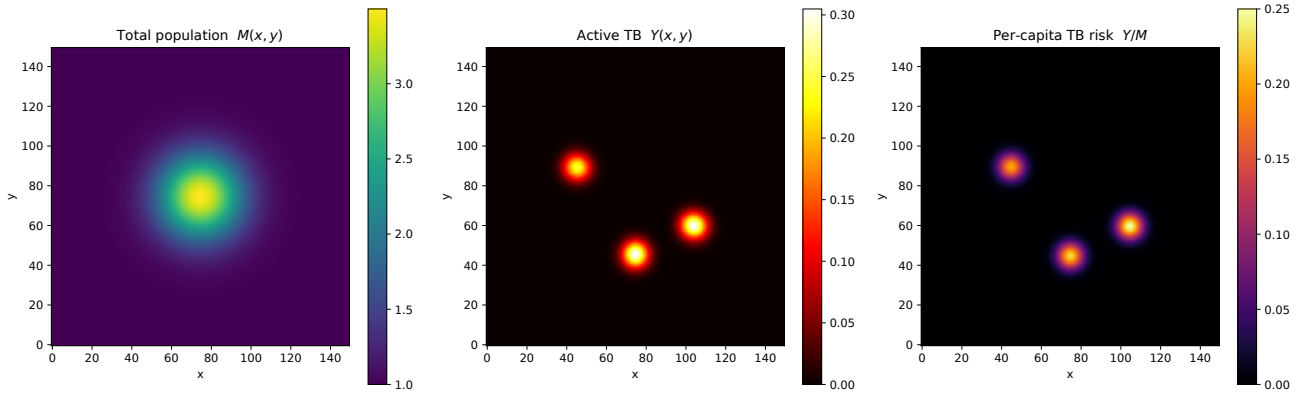

(a) (b) (c)

Figure 9. Coupling between human population density and tuberculosis risk. (a) Total human population density $M(x, y)$, (b) active tuberculosis prevalence $Y(x, y)$, (c) per-capita tuberculosis risk $Y(x, y)/M(x, y)$. The population is concentrated in a single urban center, but tuberculosis forms several spatially separated hotspots. The highest per-capita TB risk occurs outside the main population center, indicating that the emergence of TB hotspots is not driven by population density alone but by diffusion-driven epidemiological instability.

The scatter plot in Figure 10 provides quantitative insight into the mechanism of TB hotspot development. If population density is the primary factor driving tuberculosis prevalence, $M(x, y)$ and $Y(x, y)$ should have a strong monotonic connection. Figure 10 shows that TB prevalence is high across different population densities, whereas the most densely inhabited areas have consistently low levels. The model's spatial aggregation of tuberculosis (TB) is not due to population clustering, but rather to nonlinear transmission dynamics and differential mobility of epidemiological classes. This supports the diffusion-driven instability identified in Section 5.4.

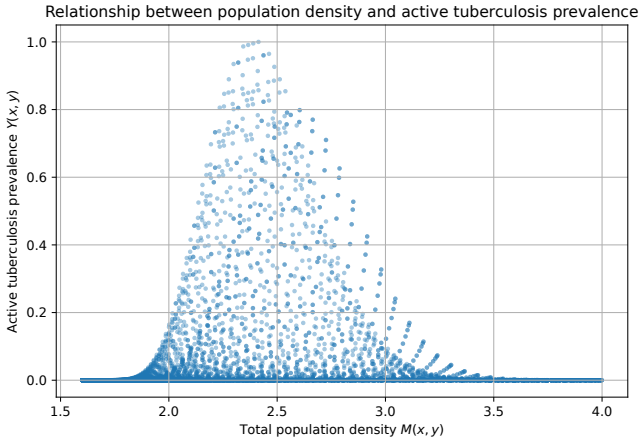

Figure 10. Relationship between total population density $M(x, y)$ and active tuberculosis prevalence $Y(x, y)$. Each point represents a spatial location (x, y).

Figure 11 shows how the spatial distribution of active tuberculosis $Y(x, y)$ changes as infectious individuals move around. Low mobility ($D_Y = 0.05$) limits TB to compact hotspots, whereas increasing D_Y results in more diffuse clusters. When infectious mobility is strong ($D_Y = 1.0$), formerly separate hotspots mix to form huge, spatially expanded regions with high TB prevalence.

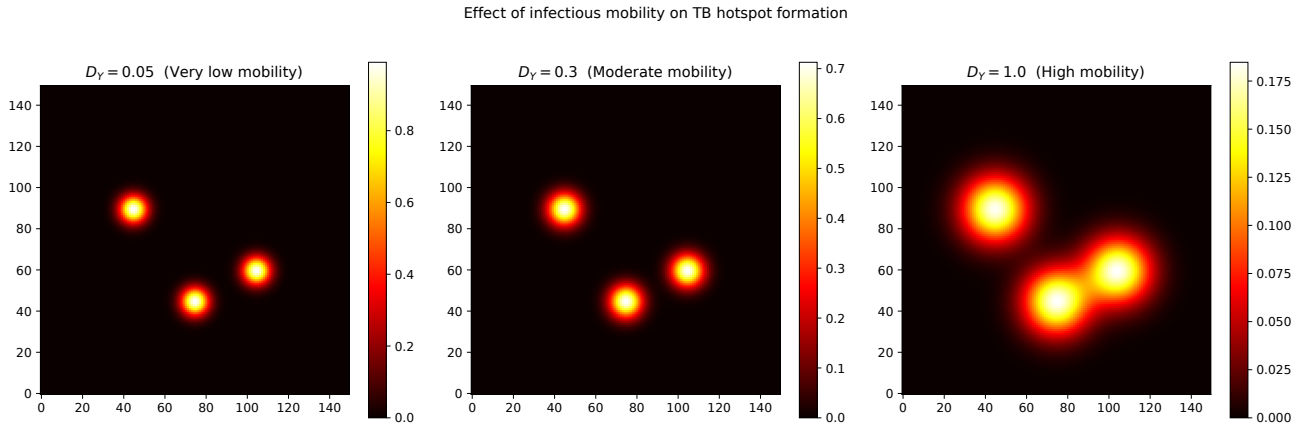

(a) (b) (c)

Figure 11. Effect of infectious mobility on TB hotspot formation. Spatial distribution of active tuberculosis $Y(x, y)$ for three values of the infectious mobility coefficient D_Y: (a) $D_Y = 0.05$ (very low mobility), (b) $D_Y = 0.3$ (moderate mobility), and (c) $D_Y = 1.0$ (high mobility).

Figure 12 shows that geographically targeted treatments lower the tuberculosis (TB) burden in densely populated areas, benefiting the majority of the population. Persistent tuberculosis reservoirs still exist in remote areas with low population density and limited access to healthcare services. The per-capita risk Y/M indicates that, although worldwide tuberculosis prevalence is decreasing, individuals living in hotspot locations still face a higher infection risk. Spatially targeted control can effectively protect urban populations, but may leave isolated or underprivileged areas vulnerable to reinfection in the long run. To address residual hotspots, supplementary techniques such as active case discovery, mobile clinics, and increased treatment coverage in rural locations should be implemented.

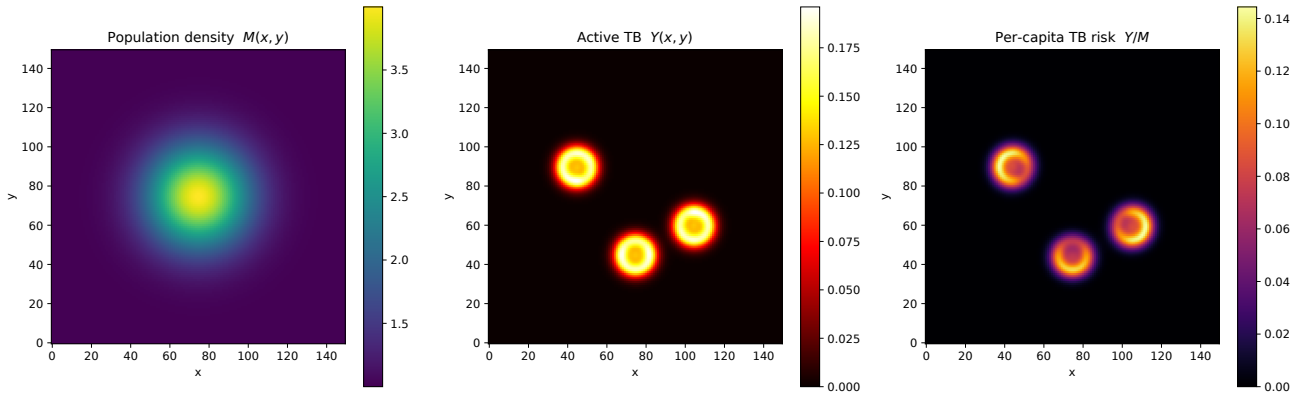

(a) (b) (c)

Figure 12. Spatial distributions of (a) total population density $M(x, y)$, (b) active tuberculosis $Y(x, y)$, and (c) per-capita TB risk $Y(x, y)/M(x, y)$ under spatially targeted intervention.

Figure 13 illustrates the quantitative dynamics of tuberculosis.

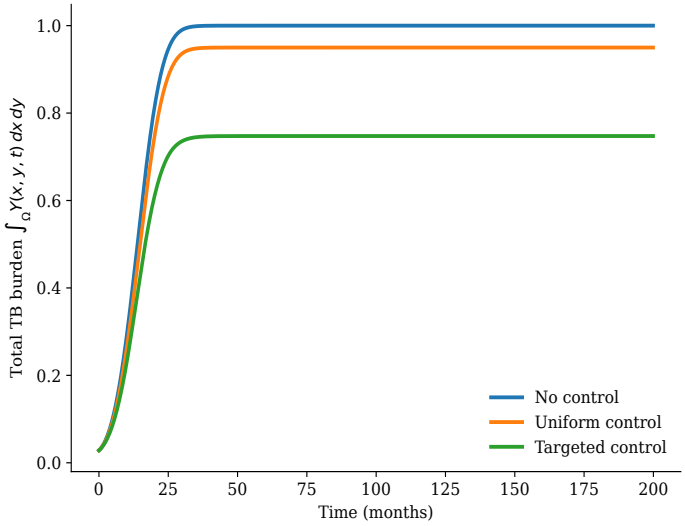

Figure 13. Total tuberculosis burden over time under three intervention strategies: no control, uniform control, and spatially targeted control. The burden is measured as the spatial integral $\int_\Omega Y(x, y, t)\, dx\, dy$, and time is reported in months.

Policy performance is evaluated in conjunction with spatial hotspot maps. Uniform control uses the same effort everywhere, reducing tuberculosis only gradually, as resources are deployed in both low- and high-risk areas. Spatially targeted control focuses interventions in high-burden areas where TB is most prevalent, resulting in a faster and longer-lasting reduction in the overall burden. The depicted quantity $\int_\Omega Y(x, y, t)\, dx\, dy$ directly measures the overall number of infectious persons in the population. The difference between the curves shows that focused control prevents more TB cases over time than an equally resourced uniform policy.

This study highlights the importance of hotspot-based interventions for improving population-level outcomes, even with conservative control assumptions.

8. Conclusions

This study sheds new light on tuberculosis dynamics by demonstrating that spatial heterogeneity and nonlinear transmission are not merely external complications, but fundamental drivers of persistent TB hotspots. We show that by combining reaction–diffusion dynamics with saturated transmission, realistic contact limitations and differential mobility between population groups can generate complex spatial structures such as localized hotspots, transmission corridors, and fragmented outbreak clusters.

This paper introduces a spatial reproduction number, R_0^S, that rigorously links tuberculosis invasion and persistence to epidemiological factors and spatial dynamics. Our results demonstrate that R_0^S can exceed the conventional reproduction number R_0, indicating that tuberculosis may persist in spatially structured populations even when well-mixed models predict elimination. This provides a mathematical explanation for why tuberculosis control is often more challenging in heterogeneous real-world settings than classical models suggest.

The diffusion-driven (Turing) instability revealed by this model identifies a powerful and previously unrecognized mechanism for TB hotspot formation. Importantly, these spatial patterns emerge naturally from the interaction of nonlinear transmission and population mobility without the need for external forcing or pre-existing environmental heterogeneity. This helps to explain why tuberculosis remains highly concentrated in locations such as densely populated urban areas, prisons, and mining communities.

Our numerical simulations further show that spatially targeted vaccination and treatment can effectively suppress these high-burden regions even when overall resources are limited. Compared with uniform intervention, hotspot-based strategies concentrate effort where transmission is highest, leading to substantially greater reductions in disease burden for the same cost. This underscores the importance of incorporating spatial structure into TB control planning rather than relying on population-averaged approaches.

Recommendations

Based on the analytical and numerical results of this study, we make the following recommendations:

- TB surveillance should be spatially explicit. Public health efforts should focus on identifying and monitoring high-transmission locations rather than relying solely on national or regional averages.
- Hotspot-based interventions should be prioritized. Targeting vaccination, screening, and

treatment resources toward high-burden communities is expected to yield greater reductions in tuberculosis transmission than uniform deployment.
- Mobility patterns should be incorporated into TB control strategies. Differences in mobility between asymptomatic (latent) and symptomatic (infectious) individuals play an important role in hotspot formation and should inform intervention planning.
- Future tuberculosis models should account for nonlinear transmission effects. Contact saturation and behavioral responses have a substantial impact on spatial dynamics and should not be overlooked in policy-relevant models.
- Spatially informed models should direct resource allocation. Mathematical models that consider transmission, migration, and heterogeneity can assist public health organizations in developing more efficient and equitable tuberculosis control programs.

Author contributions

O.J.P: Conceptualization, Investigation, Methodology, Software, Supervision, Writing–original draft; A.I.K.B.: Formal analysis, software, visualization, Funding acquisition, Project administration, Writing–review & editing; S.S.S.A.: Formal analysis, Investigation, validation, Writing–review & editing; F.H.H.A.M.: Methodology, Visualization, Validation, Writing–review & editing. All authors have read and approved the final version of the manuscript for publication.

Use of Generative-AI tools declaration

The authors declare they have not used Artificial Intelligence (AI) tools in the creation of this article.

Funding

This work was supported by the Deanship of Scientific Research, Vice Presidency for Graduate Studies and Scientific Research, King Faisal University, Saudi Arabia [Grant No. KFU262972].

Data availability

The original contributions presented in this study are included in the article. Further inquiries can be directed to the corresponding author.

Conflict of interest

The authors declare that there is no conflict of interest in the publication of the manuscript.

References

1. Global Tuberculosis Report 2022, World Health Organization (WHO), 2022.
2. Global Tuberculosis Report 2023, World Health Organization (WHO), 2023.

3. C. Dye, Global epidemiology of tuberculosis, *Lancet*, **367** (2006), 938–940. https://doi.org/10.1016/s0140-6736(06)68384-0

4. C. Dye, B. G. Williams, The population dynamics and control of tuberculosis, *Science*, **328** (2010), 856–861. https://doi.org/10.1126/science.1185449

5. K. Floyd, P. Glaziou, A. Zumla, M. Raviglione,The global tuberculosis epidemic and progress in care, prevention, and research: an overview in year 3 of the End TB era, *Lancet Respir. Med.*, **6** (2018), 299–314. https://doi.org/10.1016/S2213-2600(18)30057-2

6. S. Gupta, M. C. J. Maiden, I. M. Feavers, S. Nee, R. M. May, R. M. Anderson, The maintenance of strain structure in populations of recombining infectious agents, *Nat. Med.*, **2** (1996), 437–442. https://doi.org/10.1038/nm0496-437

7. E. L. Corbett, C. J. Watt, N. Walker, D. Maher, B. G. Williams, M. C. Raviglione, et al., The growing burden of tuberculosis: global trends and interactions with the HIV epidemic, *JAMA Intern. Med.*, **163** (2003), 1009–1021. https://doi.org/10.1001/archinte.163.9.1009

8. K. Lönnroth, E. Jaramillo, B. G. Williams, C. Dye, M. Raviglione, Drivers of tuberculosis epidemics: the role of risk factors and social determinants, *Soc. Sci. Med.*, **68** (2009), 2240–2246. https://doi.org/10.1016/j.socscimed.2009.03.041

9. N. A. Menzies, E. Wolf, D. Connors, M. Bellerose, A. N. Sbarra, T. Cohen, et al., Progression from latent infection to active disease in dynamic tuberculosis transmission models: a systematic review of the validity of modelling assumptions, *Lancet Infec. Dis.*, **18** (2018), e228–e238. https://doi.org/10.1016/s1473-3099(18)30134-8

10. E. W. Tiemersma, M. J. van der Werf, M. W. Borgdorff, B. G. Williams, N. J. D. Nagelkerke, Natural history of tuberculosis: duration and fatality of untreated pulmonary tuberculosis in HIV negative patients: a systematic review, *PLoS One*, **6** (2011), e17601. https://doi.org/10.1371/journal.pone.0017601

11. S. Díaz-Fernández, M. Aleluia, M. Saraiva, P. Soldevilla, J. B. Torrelles, R. Sharan, et al., The study of immunological markers in tuberculosis across animal models and its translation to human research, *Lab Animal*, 2026, 1–19. https://doi.org/10.1038/s41684-026-01730-9

12. C. E. Barry, H. I. Boshoff, V. Dartois, T. Dick, S. Ehrt, J. Flynn, et al., The spectrum of latent tuberculosis: rethinking the biology and intervention strategies, *Nat. Rev. Microbiol.*, **7** (2009), 845–855. https://doi.org/10.1038/nrmicro2236

13. R. M. G. J. Houben, P. J. Dodd, The global burden of latent tuberculosis infection, *PLoS Med.*, **13** (2016), e1002152. https://doi.org/10.1371/journal.pmed.1002152

14. S. Verver, R. M. Warren, N. Beyers, M. Richardson, G. D. van der Spuy, M. W. Borgdorff, et al., Rate of reinfection tuberculosis after successful treatment is higher than rate of new tuberculosis, *Am. J. Respir. Crit. Care Med.*, **171** (2005), 1430–1435. https://doi.org/10.1164/rccm.200409-1200oc

15. T. A. Yates, P. Y. Khan, G. M. Knight, J. G. Taylor, T. D. McHugh, M. Lipman, et al., The transmission of Mycobacterium tuberculosis in high burden settings, *Lancet Infect. Dis.*, **16** (2016), 227–238. https://doi.org/10.1016/S1473-3099(15)00499-5

16. C. Dye, B. G. Williams, The population dynamics and control of tuberculosis, *Science*, **328** (2010), 856–861. https://doi.org/10.1126/science.1185449

17. M. G. M. Gomes, A. O. Franco, M. C. Gomes, G. F. Medley, The reinfection threshold promotes variability in tuberculosis epidemiology and vaccine efficacy, *Proc. Biol. Sci.*, **271** (2004), 617–623. https://doi.org/10.1098/rspb.2003.2606

18. A. Sharma, A. Hill, E. Kurbatova, M. van der Walt, C. Kvasnovsky, T. E. Tupasi, et al., Estimating the future burden of multidrug-resistant and extensively drug-resistant tuberculosis in India, the Philippines, Russia, and South Africa: a mathematical modelling study, *Lancet Infect. Dis.*, **17** (2017), 707–715. https://doi.org/10.1016/S1473-3099(17)30247-5

19. A. Roy, M. Eisenhut, R. J. Harris, L. C. Rodrigues, S. Sridhar, S. Habermann, et al., Effect of BCG vaccination against Mycobacterium tuberculosis infection in children: systematic review and meta-analysis, *BMJ*, **349** (2014), g4643. https://doi.org/10.1136/bmj.g4643

20. P. Mangtani, I. Abubakar, C. Ariti, R. Beynon, L. Pimpin, P. E. M. Fine, et al., Protection by BCG vaccine against tuberculosis: a systematic review of randomized controlled trials, *Clin. Infect. Dis.*, **58** (2014), 470–480. https://doi.org/10.1093/cid/cit790

21. P. Andersen, T. M. Doherty, The success and failure of BCG—implications for a novel tuberculosis vaccine, *Nat. Rev. Microbiol.*, **3** (2005), 656–662. https://doi.org/10.1038/nrmicro1211

22. I. Abubakar, L. Pimpin, C. Ariti, R. Beynon, P. Mangtani, J. A. C. Sterne, et al., Systematic review and meta-analysis of the current evidence on the duration of protection by bacillus Calmette-Guérin vaccination against tuberculosis, *Health Technol. Asses.*, **17** (2013). https://doi.org/10.3310/hta17370

23. R. M. Anderson, R. M. May, *Infectious diseases of humans*, Oxford University Press, 1991. https://doi.org/10.1093/oso/9780198545996.002.0001

24. H. W. Hethcote, The mathematics of infectious diseases, *SIAM Rev.*, **42** (2000), 599–653. https://doi.org/10.1137/s0036144500371907

25. O. Diekmann, J. A. P. Heesterbeek, J. A. J. Metz, On the definition and the computation of the basic reproduction ratio R_0 in models for infectious diseases in heterogeneous populations, *J. Math. Biol.*, **28** (1990), 365–382. https://doi.org/10.1007/bf00178324

26. S. Gupta, M. C. J. Maiden, I. M. Feavers, S. Nee, R. M. May, R. M. Anderson, The maintenance of strain structure in populations of recombining infectious agents, *Nat. Med.*, **2** (1996), 437–442. https://doi.org/10.1038/nm0496-437

27. V. Capasso, G. Serio, A generalization of the Kermack–McKendrick model, *Math. Biosci.*, **42** (1978), 43–61. https://doi.org/10.1016/0025-5564(78)90006-8

28. M. A. Safi, S. M. Garba, Global stability analysis of SEIR model with holling type II incidence function, *Comput. Math. Methods Med.*, **2012** (2012), 1–8. https://doi.org/10.1155/2012/826052

29. G. Q. Sun, Pattern formation of an epidemic model with diffusion, *Nonlinear Dyn.*, **69** (2012), 1097–1104. https://doi.org/10.1007/s11071-012-0330-5

30. W. Wang, Backward bifurcation of an epidemic model with treatment, *Math. Biosci.*, **201** (2006), 58–71. https://doi.org/10.1016/j.mbs.2005.12.022

31. J. D. Murray, *Mathematical biology II*, Springer, 2003.

32. L. J. S. Allen, An introduction to stochastic epidemic models, In: *Mathematical epidemiology*, 2008, 81–130. https://doi.org/10.1007/978-3-540-78911-6_3
33. A. M. Turing, The chemical basis of morphogenesis, In: *The essential turing*, Oxford University Press, 1952.
34. M. Haque, J. Chen, T. Bi, H. Chen, J. Chen, Y. Wang, et al., Pattern formation in a predator–prey model on network and non-network environments, *Chaos, Soliton. Fract.*, **209** (2026), 118486. https://doi.org/10.1016/j.chaos.2026.118486
35. L. Chang, S. Gao, Z. Wang, Optimal control of pattern formations for an SIR reaction–diffusion epidemic model, *J. Theor. Biol.*, **536** (2022), 111003. https://doi.org/10.1016/j.jtbi.2022.111003
36. S. Lenhart, J. Workman, *Optimal control applied to biological models*, New York: Chapman and Hall/CRC, 2007. https://doi.org/10.1201/9781420011418
37. W. Fleming, R. Rishel, *Deterministic and stochastic optimal control*, Springer, 1975. https://doi.org/10.1007/978-1-4612-6380-7
38. C. Castillo-Chávez, S. Blower, P. Driessche, D. Kirschner, *Mathematical approaches for emerging and reemerging infectious diseases: an introduction*, Springer Nature, 2002.
39. S. M. Blower, P. M. Small, P. C. Hopewell, Control strategies for tuberculosis epidemics: new models for old problems, *Science*, **273** (1996), 497–500. https://doi.org/10.1126/science.273.5274.497
40. H. T. Banks, K. Kunisch, *Estimation techniques for distributed parameter systems*, Birkhäuser, Boston, 1989. https://doi.org/10.1007/978-1-4612-3700-6
41. T. Kuniya, Structure of epidemic models: toward further applications in economics, *JER*, **72** (2021), 581–607. https://doi.org/10.1007/s42973-021-00094-8
42. Tanvi, R. Aggarwal, T. Kovacs, Assessing the effects of holling type-II treatment rate on HIV-TB co-infection, *Acta Biotheor.*, **69** (2021), 1–35. https://doi.org/10.1007/s10441-020-09385-w
43. P. van den Driessche, J. Watmough, Reproduction numbers and sub-threshold endemic equilibria for compartmental models of disease transmission, *Math. Biosci.*, **180** (2002), 29–48. https://doi.org/10.1016/s0025-5564(02)00108-6
44. A. K. Mengistu, P. J. Witbooi, Mathematical analysis of TB model with vaccination and saturated incidence rate, *Abstr. Appl. Anal.*, **2020** (2020), 1–10. https://doi.org/10.1155/2020/6669997
45. C. Price, A. D. Nguyen, *Latent tuberculosis*, Treasure Island (FL): StatPearls Publishing, 2024. Available from: `https://www.ncbi.nlm.nih.gov/books/NBK599527/`.
46. Global Tuberculosis Report 2020, World Health Organization (WHO), Geneva, 2020. Available from: `https://www.who.int/publications/i/item/9789240013131`.

AIMS Press